Nanopetrophysical Characterization of the Wolfcamp A Shale Formation in the Permian Basin of Southeastern New Mexico, U.S.A.

by:
Ryan Jones

Thesis
Presented to the Faculty of the Graduate School of
The University of Texas at Arlington
of the Requirement
for the Degree of

MASTER OF SCIENCE IN GEOLOGY

THE UNIVERSITY OF TEXAS AT ARLINGTON
DECEMBER 2019

Acknowledgements

I would like to thank my supervising advisor Dr. Qinhong Hu for his guidance and availability throughout the length of my graduate studies. I would also like to thank Drs. John Wickham and Mortaza Pirouz not only for serving on my committee, but also for the knowledge they shared in the classroom during my time at UTA.

I would like to thank the New Mexico Bureau of Geology and Mineral Resources (NMBGR), specifically Annabelle Lopez who was generous enough to give us access to the core library and allow us to obtain numerous samples that will continue to be tested in our lab. She provided all requested data in a timely manner and was always willing to help. Without her, this research would not have been possible. Thanks are also extended to DrillingInfo for supplying our research group with a subscription that allowed me to view production data for the wells in this study. A huge thanks goes out to Qiming Wang for the help he provided me during this research. as his guidance with testing procedures and data processing was vital to the completion of this work.

Finally, I want to send a special thanks to my wife, Emily Jones, for the constant love, support, and motivation. To my mother and step-father, Virginia and Richard Laybourne, my father, William Jones, my brother and sister, Bodie Jones and Chelsie Weems, along with their families, and my mother in law Sara Dunlap; without each and everyone of them I would not be the person I am today.

Abstract

Nanopetrophysical Characterization of the Wolfcamp A Shale Formation in the Permian Basin of Southeastern New Mexico, U.S.A.

Ryan Jones, MS

The University of Texas at Arlington, 2019

Supervising Professor: Qinhong Hu

The Permian Basin has been producing oil and gas for over a century, but the production has increased rapidly in recent years due to new completion methods such as hydraulic fracturing and horizontal drilling. The Wolfcamp Shale is a large producer of oil and gas that is found within both the Delaware and Midland sub-basins of the Permian. This study focuses on the Wolfcamp A section in the Delaware Basin which lies within southeastern New Mexico and west Texas. The most recent study performed to estimate continuous (unconventional) oil within the Delaware Basin was conducted in November 2018 by the USGS. They found that the Wolfcamp and overlying Bone Spring formations have an amount of continuous oil that more than doubles the amount found in the Wolfcamp of the Midland Basin in 2016. However, to ensure a high rate of recovery of this oil and gas it is important to understand the nano-petrophysical properties of the Wolfcamp Shale.

This study aims to obtain the nano-petrophysical properties of the Wolfcamp A shale formation in Eddy County, NM. To determine petrophysical properties such as density, porosity, permeability, pore connectivity, pore-size distribution, and wettability, various testing procedures were used on a total of 10 samples from 3 different wells in the Wolfcamp A

formation. These procedures include vacuum-assisted liquid saturation, mercury intrusion porosimetry (MIP), liquid pycnometry, contact angle/wettability, and imbibition, along with XRD, TOC, and pyrolysis evaluations. Results show that samples from two wells are carbonate-dominated and contain 0.08-0.25% TOC, while the third well shows higher amounts of quartz/clay with 1.56-4.76% TOC. All samples show a high concentration of intergranular pores, and two dominant pore-throat sizes of 2.8-50 nm and >100 nm are discovered. Permeability and tortuosity values in the 2.8-50 nm pore network range from 2.75-21.6 nD and 375-2083, as compared to $8.85 10^{3}$ -5.44×10^{5} nD and 5.49-295 in the >100 nm pore network. Average porosity values range from 0.891-9.98% from several approaches, and overall wettable pore connectivity is considered intermediate towards deionized water (hydrophilic fluid) and high towards DT2 (n-decane:toluene=1:1, a hydrophobic fluid).

Table of Contents

List of Figures

List of Tables

List of Abbreviations

CM: Centimeter

DIW/ DI Water: Deionized Water

DT2: **N-decane:t**oluene at 2:1 in volume

FE-SEM: Field emission-scanning electron microscopy

HI: Hydrogen Index.

McF: Thousand cubic feet (gas)

MIP: Mercury intrusion porosimetry

um: Micrometer

nD: nano-darcy

nm: Nanometer

OI: Oxygen Index

PI: Production index

SANS: Small-angle neutron scattering

THF: Tetrahydrofuran

TOC: Total organic carbon

XRD: X-Ray diffraction

Chapter 1: Introduction

Over the last several years, the Wolfcamp Shale in the Delaware Basin has been found to be one of the largest unconventional plays in the world. Production within the Delaware Basin has increased and therefore the need for more information on the nano-petrophysical properties of the rock. The Wolfcamp Shale is an organic-rich formation that extends in the subsurface under all three sub-basins of the Permian Basin: the Delaware Basin, Midland Basin, and Central Basin Platform (Figure 1). The formation is divided into four sections (A, B, C, and D) which show different characteristics in terms of lithology, fossil content, porosity, total organic carbon content, and thermal maturity; A and B are the sections most commonly drilled (Gaswirth, 2017). A recent study completed by the USGS showed that the Delaware Basin's Wolfcamp and Bone Spring formations to contain an estimated 46.3 billion barrels of oil, 281 trillion cubic feet of natural gas, and 20 billion barrels of natural gas liquids, more than twice the amount of the heralded Midland Basin side. Given statistics like these, the exploration companies will undoubtedly ramp up their efforts to recover as much oil and gas as possible, but numerous petrophysical studies (properties of rock and fluids and their interactions) need to be performed to aid in that effort. For this study, 10 core samples from 3 wells were chosen within the Wolfcamp A formation and subjected to a slew of testing procedures to ultimately obtain a better understanding of pore structure about, and fluid flow through, the formation.

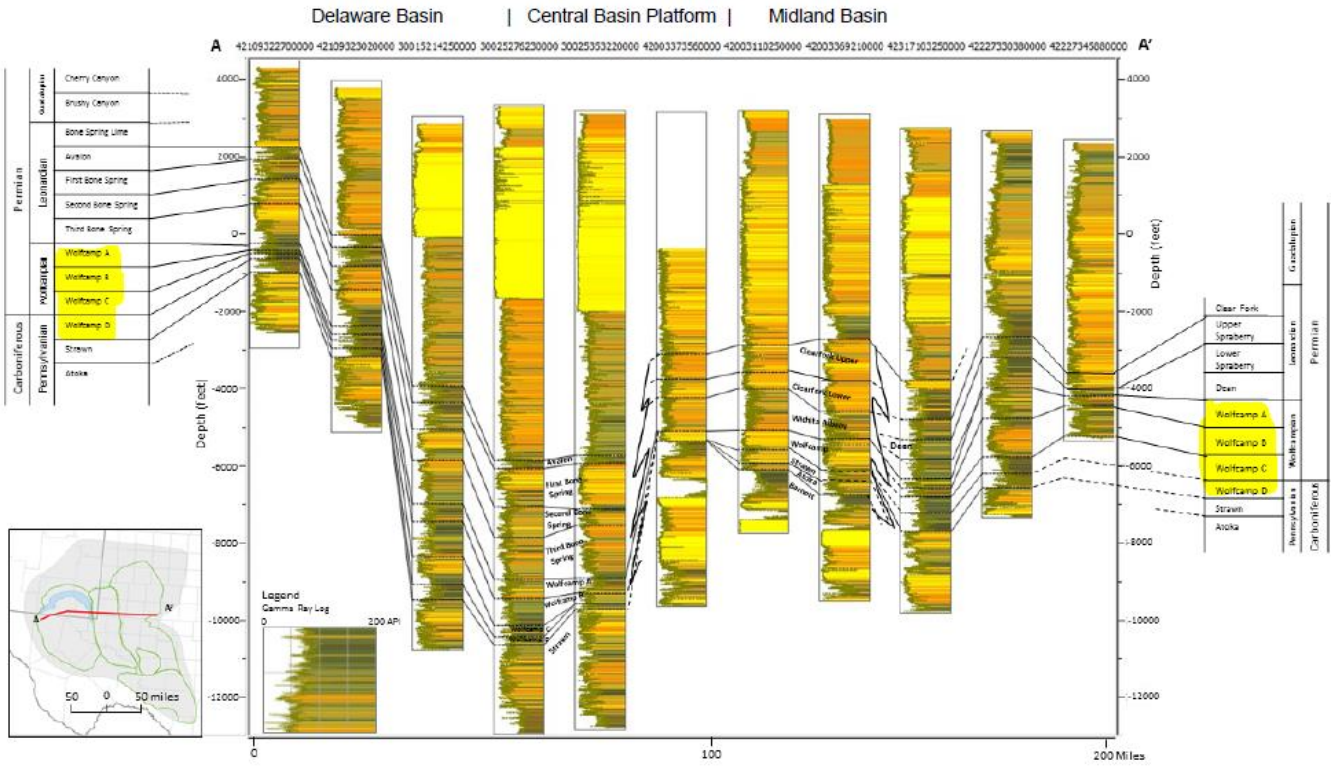

Figure 1: East-West Cross Section Through the Permian Basin (EIA, 2018)

Chapter 2: Geologic Background

2.1 Geologic setting

The Permian Basin is a large sedimentary basin located in West Texas and Southeast New Mexico. As one of the biggest basins in the world, it is present in 52 counties and extends throughout an area of more than 75,000 square miles. The Permian Basin began its development in the middle Carboniferous as an open marine area called the Tobosa Basin (Galley, 1958). At present day, the Permian Basin is an asymmetrical, northwest to southeast-trending sedimentary system bounded by the Marathon-Ouachita orogenic belt to the south, the Northwest shelf and Matador Arch to the north, the Diablo platform to the west, and the Eastern shelf to the east (Gardiner, 1990; Ewing, 1991; Hills, 1985). Within the Permian Basin there are two large sub-

basins, the Midland and Delaware, along with the Central Basin Platform which separates them (Figure 2).

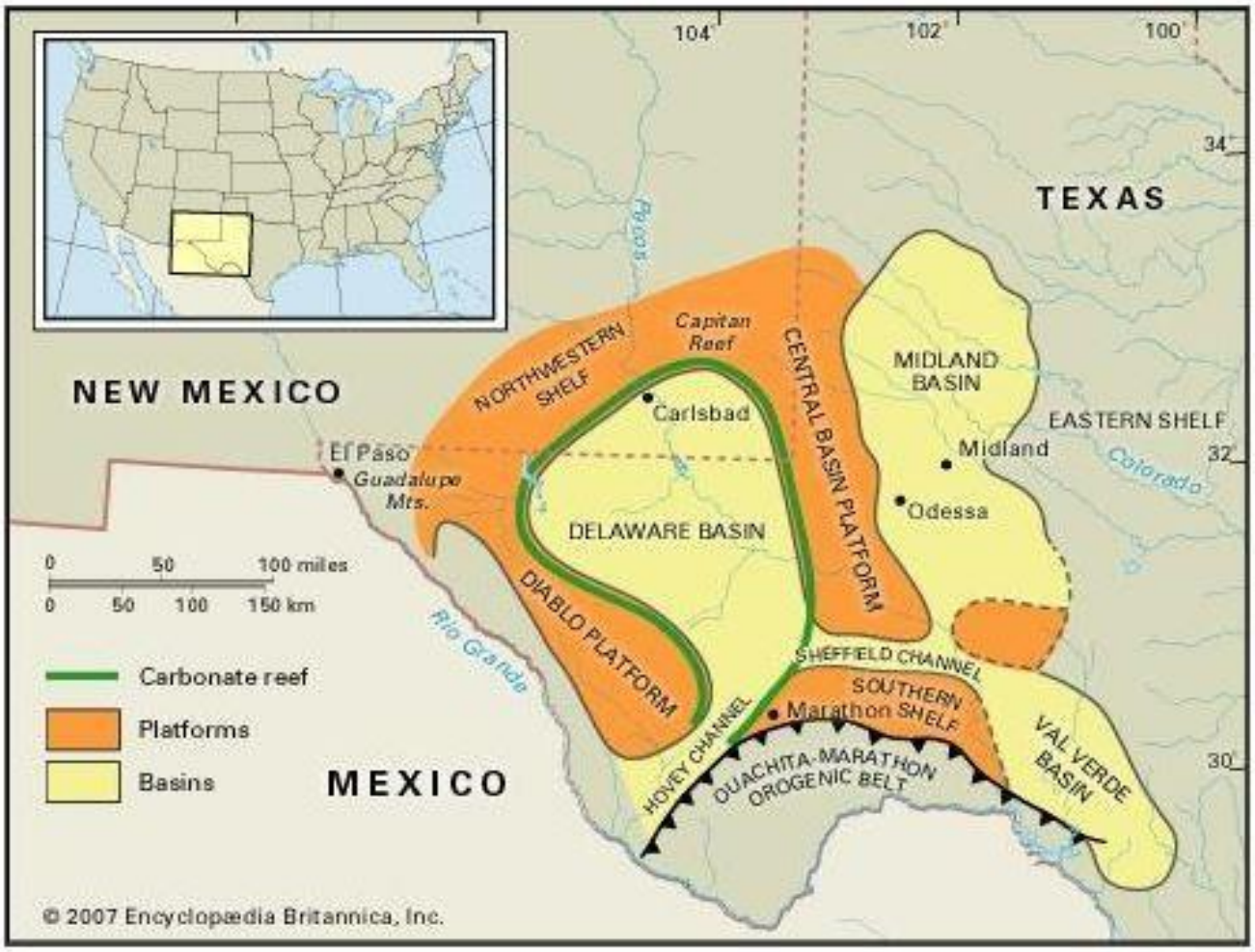

Figure 2: Permian Basin Map (https://www.britannica.com/place/Permian-Basin)

The largest portion of separation between these sub-basins was during the Pennsylvanian and Wolfcampian time when a rapid subsidence was occurring in both basins while an uplift of the Central Basin Platform was happening simultaneously. The end of the Wolfcampian marked the

time where the rapid subsidence stopped, but the subsidence was still occurring at a slower rate until the end of the Permian (Oriel et al., 1967; Robinson, K., 1988; Yang and Dorobek, 1995).

The samples acquired for this study came from the Delaware Basin which is bounded to the north by the Northwestern shelf, to the south by the Marathon-Ouachita fold belt, to the west by the Diablo Platform, and to the east by uplifted areas of the Central Basin Platform (EIA, 2018).

2.2 Stratigraphy

The Delaware Basin contains numerous rock formations that range from Pennsylvanian to Guadalupian in age (Figure 3). For the purpose of this study, the focus will be on the stratigraphy of the Wolfcamp formation. The Wolfcamp formation is found throughout the entire Permian Basin and was deposited during late Pennsylvanian through late Wolfcampian time. It consists of mostly organic-rich shale and argillaceous carbonates intervals near the basin edges (EIA, 2018). The thickness and lithology vary throughout the formation, and the depth increases towards the Central Basin Platform. The Wolfcamp formation is a stacked play and broken up into four sections, A, B, C, and D (Gaswirth, 2017). Average porosity values tend to be between 2% and 12% and permeability averages around 10 millidarcies (mD). Wolfcamp A and B are the most drilled portions of the formation, and the samples acquired for this work lie within the Wolfcamp A section. In these regions the thickness can be more than 1,000 feet, subsea depth to the formation top is more than 3,000 feet, neutron porosity ranges from 4% to 8%, and estimated total organic carbon ranges from 1% to 8% (EIA, 2018)

Delaware Basin

Period	Epoch	Stage
Permian	Guadalupian	Bell Canyon
		Cherry Canyon
		Brushy Canyon
	Leonardian	Bone Spring Lime
		Avaon Sand
		First Bone Spring
		Second Bone Spring
		Third Bone Spring
	Wolfcampian	Wolfcamp A
		Wolfcamp B
		Wolfcamp C
Carboniferous	Pennsylvanian	Wolfcamp D
		Strawn
		Atoka

Figure 3: Stratigraphic Column of Delaware Basin (EIA, 2018)

Chapter 3: Methods

3.1 Sample Acquisition & Preparation

After deciding to focus my research on the Wolfcamp Formation of Eddy County, NM in the Delaware Basin I contacted Annabelle Lopez, the Petroleum Information Coordinator at the New Mexico Bureau of Geology & Mineral Resources (NMBGR). Upon my request she sent an Excel spreadsheet containing information available for the samples they had in their core library located at the New Mexico Institute of Mining and Technology in Socorro, NM. Based on that information I downloaded well completion reports from the New Mexico Oil Conservation Division (NMOCD) website which included formation tops. This is important because the NMBGR and the NMOCD do not label their Wolfcamp core samples with the typical A, B, C, and D sections like most recent publications on the Permian Basin do. Since these determinations are not available, I decided to choose wells with available core samples that lie within a few feet of the Wolfcamp formation tops to ensure that I was working within the Wolfcamp A section. I also factored in sample size availability, close proximity of the wells, and production information while determining which wells I should choose. Of the wells that met that criteria, I chose the following three: 1) Richard Knob AEX State (API: 30-015-26073), 2) Foothills AGH State (API: 30-015-26062), and 3) Fed BH (API: 30-015-23355). Once Annabelle confirmed their availability, I took a flight to New Mexico to obtain my samples. Upon arrival I was given access to the core buildings to find the boxes containing the specific core intervals of interest. From the three wells I was able to secure 11 samples in total, eight samples of half-core from Richard Knob AEX State and Foothills AGH State (four each for a well), and three whole-core samples from Fed BH well. After returning to UTA, each sample was assigned a unique sample ID which includes abbreviated well name, depth of the sample, and weight (Table 1).

Well Name	Sample ID	Depth (ft.)	Mass (g)
Foothills AGH State	1F-4648	4648	725.33
Foothills AGH State	1F-4672	4672	442.48
Foothills AGH State	1F-4693	4693	509.25
Foothills AGH State	1F-4705	4705	497.93
Fed BH	1FBH-6490	6490	905.60
Fed BH	1FBH-6513	6513	1540.70
Fed BH	1FBH-6536	6536	1076.50
Richard Knob AEX State	2RK-4899	4899	585.02
Richard Knob AEX State	2RK-4939	4939	497.44
Richard Knob AEX State	2RK-4966	4966	441.00
Richard Knob AEX State	2RK-4981	4981	474.52

Table 1: Well Name, Unique Sample ID, Depth, and Mass of Samples recorded

Once the IDs were assigned, pictures of the whole sample, a ruler for scale, and sample ID (Figure 4) were taken with a digital camera. Then the whole samples were prepared for vacuum saturation with DI (deionized) water and tested over the next several weeks. During the initial vacuum saturation testing, sample 1FBH-6536 was completely disaggregated therefore I made the decision to exclude it from further testing. Following this first round of vacuum saturation with DI water, core plugs (1 inch in diameter and several centimeters in length) were taken from the original samples. Two plugs were obtained from each of the depth intervals in the 1F and 2RK well samples. These were parallel to the bedding plane thus given the ID of 1P and 2P. For the 1FBH well samples, one long plug was able to be obtained from the parallel bedding plane on both of them, those were then cut into three short ones and given the IDs of 1PA, 1PB, and 1PC. One plug from each of the 1FBH samples was also taken at the direction transverse to the bedding plane thus given the ID of 1T. Following this, I was able to cut at least 15 1 cm-

sided cubes per sample. Of these cubes, three from each sample were assigned as X, Y, and Z, two from each sample were cut in half, two from each sample were cut into thirds, and one from each sample was epoxied for imbibition tests.

a. 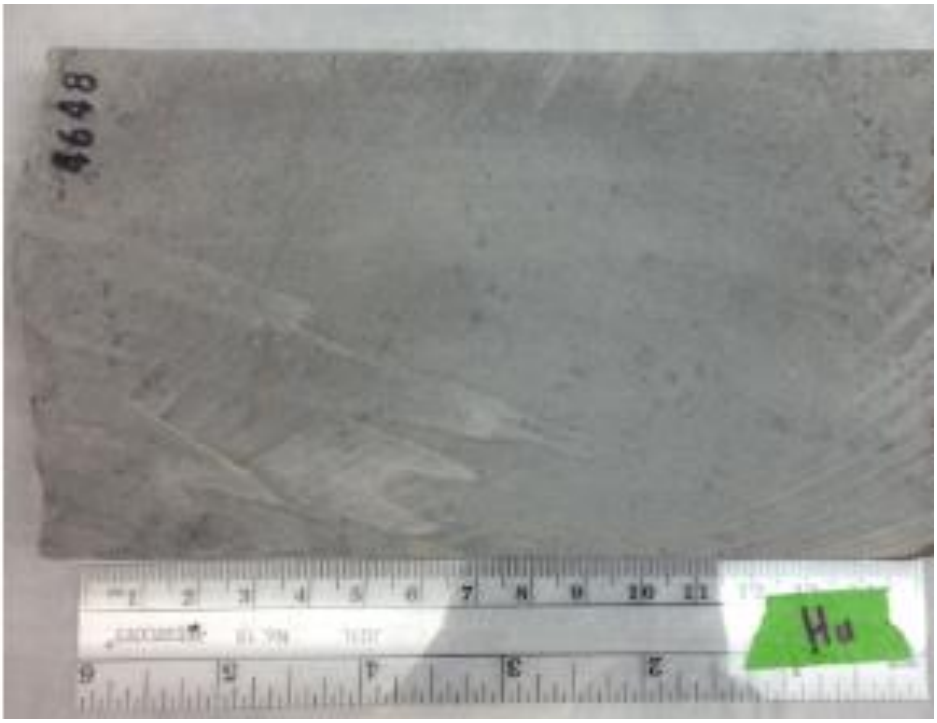

b.

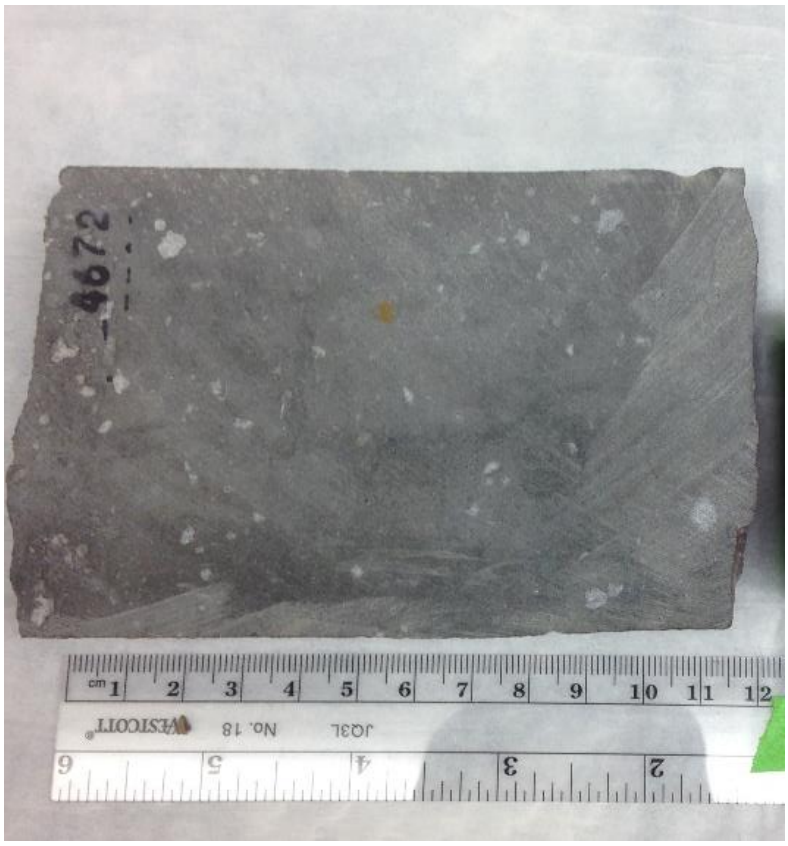

c.

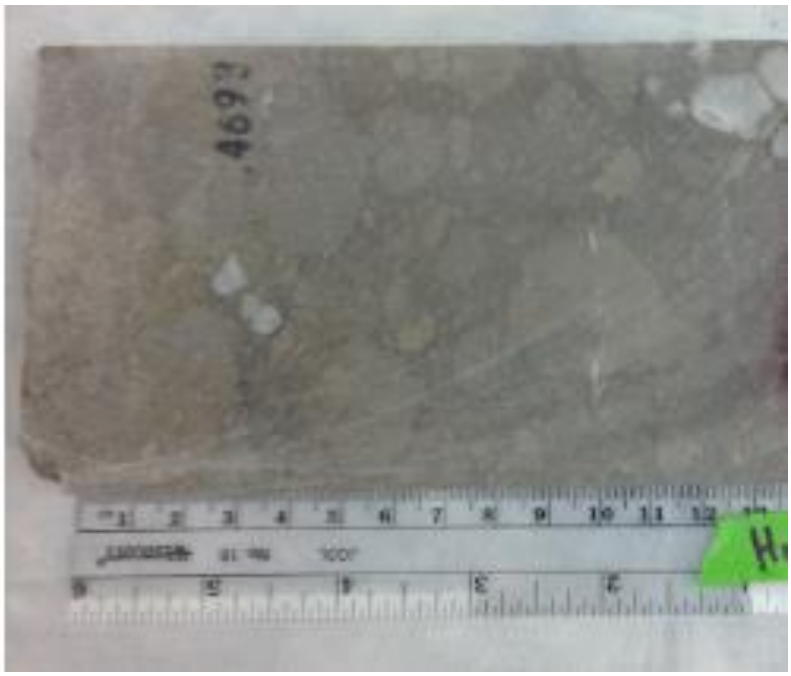

d. 

e. 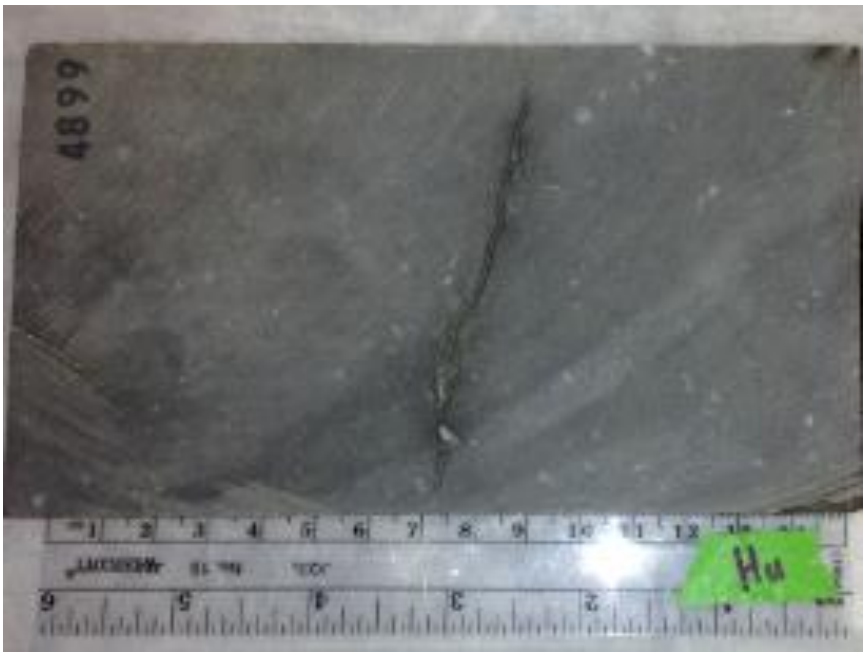

f. 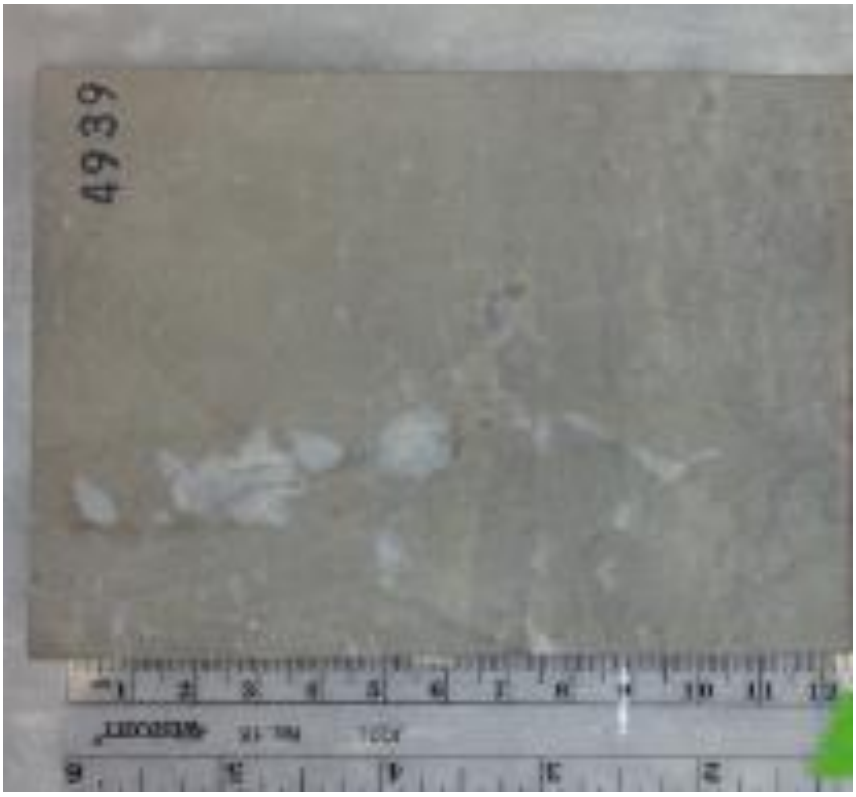

g. 

h. 

i. 

j. 

Figure 4: (a-j) Whole sample images

Following this the rest of sample fragments was reduced by crushing them with the large pestle and mortar, then separating them by stacking sieves #8/#12, #12/#20, #20/#35, #35/#80, #80/#200, and <#200 to produce sizes of GRI+ (Gas Research Institute), A, GRI, B, C, and powder (these names are locally used in the research laboratory of Dr. Hu), respectively. Whole samples, core plugs, and X-Y-Z cubes were all subjected to vacuum saturation tests using DI water. The Y cube was subsequently subjected to vacuum saturation with tetrahydrofuran (THF), and the Z cube with DT2 (a mixture of 2:1 in volume of n-decane and toluene, as a model oil from moderately mature source rocks). Liquid pycnometry with DI water, DT2, and THF was performed on sizes GRI+, A, B, and C. The X cube, thin slabs, and GRI were sent to the collaborating labs in China for MIP, contact angle, and nitrogen physisorption tests. Finally, the

powder size was sent to the Shimadzu Center at UTA for XRD analysis and GeoMark in Humble, Texas for TOC & pyrolysis analyses. Sample size designation can be seen in and a photo of the representative sizes can be seen in Table 2.

Size Designation	Sieve mesh	Size Fraction (diameter)	Equivalent spherical diameter (µm)
Cylinder/Plug		2.54 cm dia ; any height (e.g 3 cm)	(24394)
Cube		1.0 cm	6204
GRI+	#8 to #12	1.70 - 2.36 mm	2030
Size A	#12 to #20	841 - 1700 µm	1271
GRI	#20 to #35	500 - 841 µm	671
Size B	#35 to #80	177 - 500 µm	339
Size C	#80 to #200	75 - 177 µm	126
Powder	< #200	< 75 µm	< 75

Table 2: Sample size designation

3.2 XRD, TOC, and Pyrolysis

X-Ray Diffraction (XRD) analysis is used to determine the mineral composition of the samples and their respective weight percentages. XRD analysis was carried out on 10 samples using the Shimadzu MAXimaX XRD-7000 machine. Methods and procedures for this process can be found in Appendix A. With the information provided by these analysis, bulk mineral percentages were calculated and plotted on a lithofacies ternary diagram.

Total organic carbon (TOC) and pyrolysis analyses were performed on 10 samples, using the powder size fraction of <75 μm, at GeoMark Research in Humble, Texas. Methods and procedures are attached in Appendix B. For determining the amount of total organic carbon within the samples GeoMark used the LECO TOC instrument and for pyrolysis analysis the HAWK program was used. Data provided from the pyrolysis analysis includes S1, S2, S3, T_{max}, HI (hydrogen index), OI (Oxygen Index), Vitrinite Reflectance (Calculated using T_{max}), Normal Oil Content, and Production Index. S1 represents the residual hydrocarbons left within the rock, S2 indicates the remaining hydrocarbon generation potential within the rock, S3 shows the carbon dioxide yield during the breakdown of kerogen (CO_2 remaining within the sample), and T_{max} is the maximum point of temperature during hydrocarbon generation during S2 analysis.

3.3 Vacuum Saturation

Vacuum saturation is a method used to find edge-only accessible porosity, grain density, and bulk density. This procedure is done using the custom-designed apparatus shown in Figure 5 and in combination with the use of the Archimedes Principle. Given the large size of the chamber this testing procedure can be performed on various sample size including whole core, plugs, and $1cm^3$ cubes. Once the following procedure is completed, grain density, bulk density, and porosity can be calculated

Figure 5: Vacuum Saturation Apparatus

Procedure for Vacuum Saturation

After the air-dry weight was taken, the sample was put into the oven of 60 ^{o}C and dried for 48 hours, then weighed again before being placed into the chamber. Once the chamber was sealed, the evacuation began for approx. 6-8 hours and pressure reached <0.2 Torr. After the initial evacuation, for DIW runs CO_2 was introduced into the chamber for 30 minutes in order to replace residual air in the pore spaces, then a second evacuation was run overnight. Next the fluid (DIW, DT2, or THF) was released into the chamber until the samples were fully immersed.

A pressured CO_2 at 50 psi was introduced into the chamber for another 30 minutes in order to push fluids into the pore spaces of submerged samples, then after letting the samples submerged for approximately 3-4 hours the chamber was opened to the atmosphere. Weights in air and in fluid (using the Archimedes principle) were taken twice and recorded for each sample and then samples were placed back into the oven to dry for more than 48 hours. After drying, the final weights were recorded to check any sample loss from the processing. Given the weights before and after saturation, the total mass of fluid saturated into the samples can be calculated.

3.4 Mercury Intrusion Porosimetry (MIP)

The MIP analysis was performed using the Micrometics Autopore IV 9520 machine (Figure 6). This analysis can measure multiple pore structure characteristics such as bulk density, grain density, porosity, pore surface area, and pore-throat size distribution while tortuosity and permeability can be inferred given the MIP data (Hu et al., 2015). The process as described by (Hu et al., 2015) is as follows, "Each sample was oven dried at 60°C for at least 48 h to remove the moisture in pore spaces, then cooled to room temperature in a desiccator. Before the introduction of liquid mercury, samples were evacuated to 6.7 Pa (99.993% vacuum). The highest pressure produced by the porosimeter is 60,000 psia (413 MPa), corresponding to a pore throat diameter of about 3 nm via the Washburn equation." Given that mercury is a non-wetting fluid for most rock samples it will not invade the pore spaces unless a pressure is applied; the higher the pressure is applied, the smaller the pores that can be invaded (Gao and Hu, 2013). The inverse relationship of pore diameter invaded to pressure applied is described by the afore-mentioned Washburn equation (Equation 1; Washburn 1921).

$$\Delta P = -\frac{2\gamma \cos\theta}{R}$$

(Equation 1)

Where,

ΔP- Difference in pressure (psia);

γ- Surface tension for mercury (dynes/cm);

θ- Contact angle between porous media and mercury (degrees);

R- Pore throat radius (μm).

Recent developments by Wang et al. (2016) have led to a modification of the original Washburn equation which is shown in Equation 2. They found that "Considering the variation of contact angle and surface tension with pore size improves the agreement between MICP and adsorption-derived pore size distribution, especially for pores having a radius smaller than 5 nm."

$$\Delta P = -\frac{2\gamma_{Hg}(R)\cos\theta_{Hg}(R)}{R}$$

(Equation 2)

As previously mentioned, along with the calculation of bulk density, grain density, porosity, pore surface area, and pore-throat size distribution, tortuosity and permeability can also be obtained with the data received from the MIP method. The permeability is calculated using the Katz and Thompson equation (Equation 3; Katz and Thompson, 1986; 1987).

$$k = \frac{1}{89}(L_{\max})^2 \left(\frac{L_{\max}}{L_c}\right) \varphi S(L_{\max})$$

(Equation 3)

Where,

k: Absolute permeability (μm^2);

L_{max}: Pore throat diameter at the maximum hydraulic conductance (µm)

L_c: length (µm) of the pore throat diameter corresponding to the threshold pressure

ϕ- Porosity of the sample (%);

$S(L_{max})$- Mercury saturation at L_{max} (Gao and Hu, 2013).

Tortuosity was calculated from the MIP data using Equation 4 (Hager, 1998; Webb, 2001; Hu et al., 2015)

$$\tau = \sqrt{\frac{\rho}{24k(1+\rho V_{tot})}\int_{\eta=r_c,min}^{\eta=r_c,max}\eta^2 f_v(\eta)d\eta}$$

(Equation 4)

Where,

τ: Effective tortuosity (dimensionless);

ρ : sample density ($g/(cm^3)$);

V_{tot}: Total pore volume (mL/g);

$\int_{n=rc,min}^{n=rc,max}$ η2 fv (η) dη: Pore throat volume probability density function

Figure 6: Micrometrics Autopore IV 9520

3.5 Contact Angle

Contact angle measurements are used to quantify the wettability of a sample when the surface is exposed to various fluids including DIW, API (American Petroleum Institute) brine, 20% THF in DIW, 20% isopropyl alcohol (IPA) in DIW, and DT2. The fluids administered during this procedure all represent different conditions. The DT2 is a representation of a hydrophobic fluid, the DIW is a representation of a hydrophilic fluid, the IPA is a representation of an amphiphilic fluid, and the API brine is a representation of fluid at reservoir conditions (Wang, 2019). The contact angle is measured based upon how much of the fluid spreads along the sample's surface in a given amount of time. A low contact angle corresponds to wetting fluid to the surface while and high angle corresponds to a non-wetting fluid (Figure 7). The machine used for this test, the USA KINO SL200KB (Figure 8), administers a droplet of fluid onto the sample surface and captures images to measure the angle created by the contact of the sample surface and the fluid.

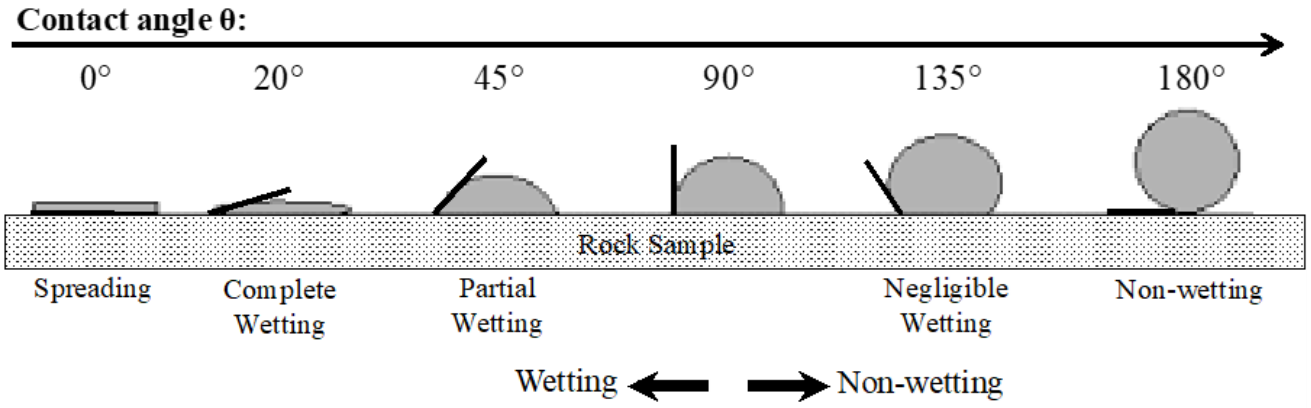

Figure 7: Contact angle schematic (modified after Majeed, 2014).

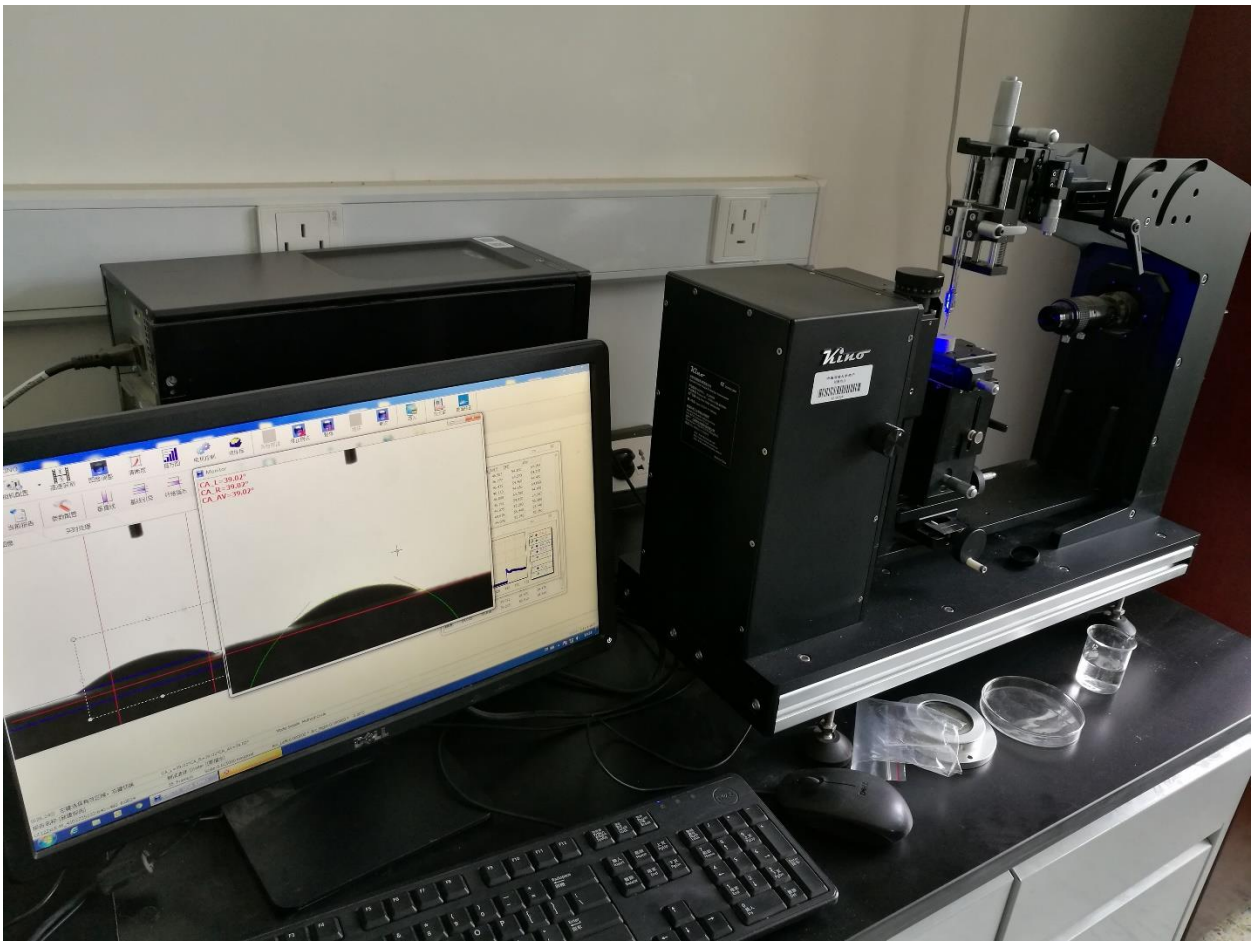

Figure 8: SL200KB Optical Contact Angle & interface tension meter

3.6 Spontaneous Imbibition

The imbibition test performed uses the Radwag AS 60/220.R2. balance (Figure 9) to qualitatively assess the pore connectivity and wettability in a sample. During spontaneous imbibition, the nonwetting air is displaced by a wetting fluid due to capillary forces (Gao and Hu, 2011). Imbibition rate, being a capillary pressure dominated process, is strongly related to the properties of fluids, porous media, and the fluid-rock interactions (Yang et al., 2017). During the testing, a sample is exposed to two types of fluid, DIW and DT2. Depending on the results we can infer if the sample is either oil- (DT2) or water-wet (DIW). For the imbibition process with a wetting fluid into well-connected pore networks, the total amount of liquid imbibed can be calculated with the Handy Equation (Handy, 1960; Yang et al., 2017; Equation 5).

$$V_{imb} = \left(\left[\left(\frac{2PcKw\varphi SwAc}{\mu_w}\right) t\right]^{0.5}\right. \qquad \text{Equation 3-5}$$

Where,

V_{imb}: total volume of water imbibed, cm^3

P_c: capillary pressure, Pa

K_w: the effective permeability of the porous medium to a wetting fluid, cm^2

A_c: imbibition cross-sectional area, cm^2

t: imbibition time, s

S_w: water saturation, %

μ_w: fluid viscosity, Pa×s

φ: sample porosity (fraction)

A)

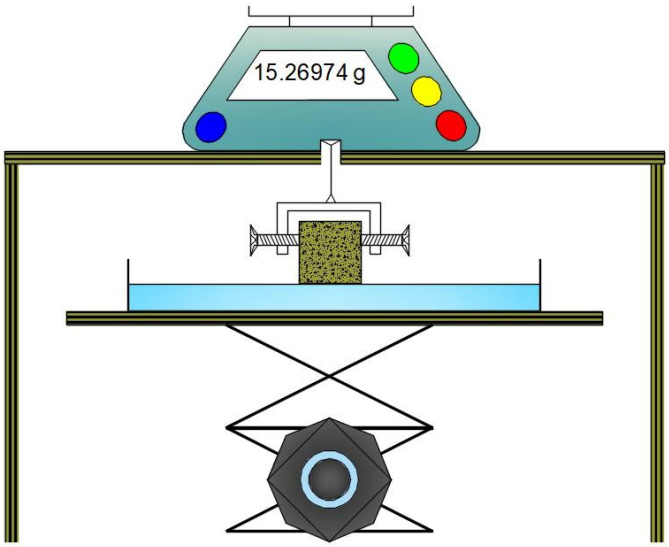

B)

Figure 9: A) photo and, B) Schematic of imbibition apparatus (Wang, 2019)

Procedure for Spontaneous Imbibition

This procedure involves using a 1 cm^3 cube that has been epoxied on all sides except for two that are opposite of each other. The sample was placed in a 60-degree oven and dried for

more than 48 hours to ensure there was no fluid within the pore space. Following a brief cooling period, numerous weights were taken including the dry weight of the sample, the weight of the sample holder, weight of sample and holder together, and the weight of the dish and solution being used (DIW or DT2). Next, the sample was hooked up to the balance and immersed into the fluid. The duration of the test and balance reading intervals, which help determine the amount of fluid uptake, depend on the fluid being used. For DI water, the test ran for 24 hours and had balance reading intervals of 1 sec for the first two minutes, 30 sec for the following 1 hr, 120 sec for the following 5 hrs, then 300 sec for the remaining portion of the run. For DT2, the intervals remained the same, but the duration of the test was only 6 hours, as DT2 wets the sample much better than DIW from the contact angle analyses. Following the procedure, the weights listed above were taken again as well as checking the other side of the cube for traces of fluid.

3.7 Liquid Pycnometry

Liquid pycnometry is a method used to find the "apparent" bulk density of a porous dry sample in three different fluids (DIW, DT2, and THF). For initially dry core samples, plugs and cubes, we used a balance and custom-designed basket submerged in a fluid. For smaller sample size fractions (GRI+, A, GRI, B, and C), we used a calibrated pycnometer. Depending on the size of the pycnometer a certain amount of sample was used. For a 5-mL pycnometer, 1 gram was sufficient and for a 10 mL we used 2 grams. The samples were placed in the oven of 60 degrees to dry for approximately 48 hours, then weighed out 2 g with the precision of 0.0001 g. Following this, the weights of the pycnometer with dry sample, pycnometer with sample and fluid, then the pycnometer with only fluid were taken. After doing this test for all sizes across a sample, the "apparent" bulk density can be calculated and compared with calculated densities from other procedures such as vacuum saturation and MICP for cubic samples. More

importantly, these different sample sizes and fluids for the same sample will provide an understanding on the sample size-dependent porosity, compounded with wettability.

Chapter 4: Results

4.1 X-Ray Diffraction (Mineralogy)

The mineralogical composition and lithofacies description of these samples from XRD analyses are shown in Table 3. For the purpose of this study we use a shale classification ternary diagram that is modified from Schlumberger (2014) (Figure 10). With this diagram the three major mineral groups of quartz/feldspar (QF), carbonates, and clays are used to determine the lithofacies description. The minerals that make up these groups are as follows, for QF we include silica and albite, for carbonate we include calcite and dolomite, and for clays we include illite, montmorillonite, and clinochlore. Other mineral phases found within the samples include anhydrite, pyrite, and ulvospinel. Pie charts were also included to clearly display their mineral percentages (Figure 11A-J).

Samples 1F 4648-4705 from the 1 Foothills AGH State well contains carbonate percentages ranging from 84.1 to 92.1%, QF percentages from 1.3 to 3.5%, no clay content, and anhydrite percentages from 4.0-14.6%. Samples 2RK 4899-4981 from the 2 Richard Knob AEX State well possess carbonate percentages ranging from 87.3-98.1%, QF percentages from 0.3-3.9%, no clay content, and anhydrite percentages from 3.5-11.7%. Samples 1FBH 6490 and 6513 from the 1 Fed BH well have carbonate percentages of 6.4 and 73%, QF percentages of 38.6 and 16.9%, clay content of 28.7 and 9.5%, respectively; in addition, 1FBH 6490 contains 22% anhydrite. When these numbers are factored into the ternary chart, with anhydrite and trace minerals excluded, the eight samples of 1F 4648-4705 and 2RK 4899-4981 all plotted as

carbonate-dominated lithotype. In addition, sample 1FBH 6490 is shown as a clay- rich siliceous mudstone and 1FBH 6513 as a silica-rich carbonate mudstone.

	Quartz & Feldspar		Carbonate		Sulfate	Sulfide	Oxide	Clay			
	Quartz	Albite	Calcite	Dolomite	Anhydrite	Pyrite	Ulvospinel	Illite	Montmorillonite	Clinochlore	Lithofacies Description
Sample ID	Weight Percent (wt%)										
1F 4648	2	0.3	66.8	18.2	12.7						Carbonate dominated lithotype
1F 4672	1.3		12	72.1	14.6						Carbonate dominated lithotype
1F 4693	1.8			90.4	7.8						Carbonate dominated lithotype
1F 4705	3.5		1.2	90.9	4	0.4					Carbonate dominated lithotype
1FBH 6490	35.5	3.1	0.6	5.8	22	3.3	1	26.3	1.1	1.3	Clay- rich siliceous mudstone
1FBH 6513	16.5	0.4	72.4	0.6			0.6	8.2	0.5	0.8	Silica-rich carbonate mudstone
2RK 4899	1		0.2	87.1	11.7						Carbonate dominated lithotype
2RK 4939	0.3		18.9	77.3	3.5						Carbonate dominated lithotype
2RK 4966	3.1	0.8	68.9	26.5		0.7					Carbonate dominated lithotype
2RK 4981	1.9		94.4	3.7							Carbonate dominated lithotype

Table 3: Mineral composition of samples in weight percent (wt.%)

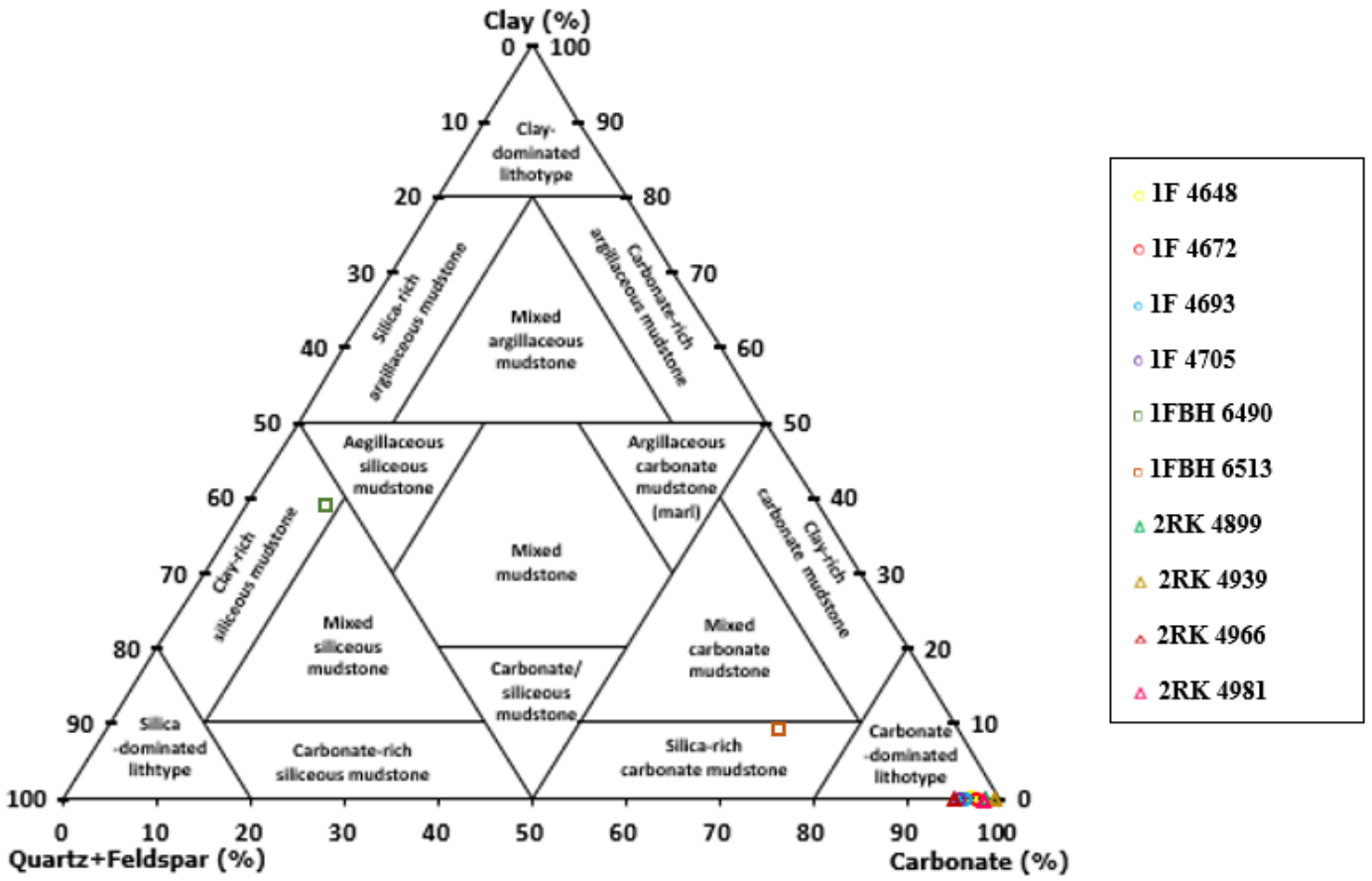

Figure 10: Ternary shale classification diagram for Wolfcamp A samples (modified from Schlumberger, 2014)

A

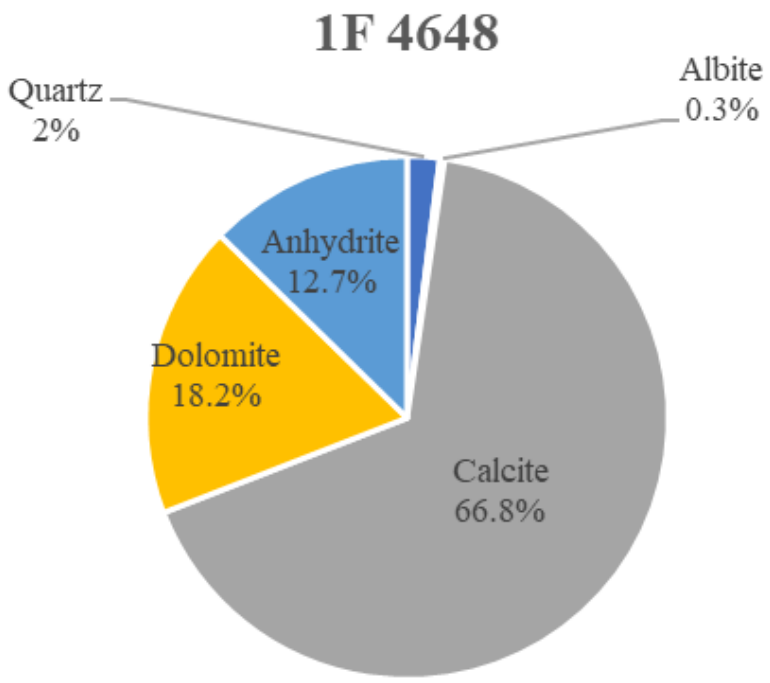
1F 4648
Quartz
2%
Albite
0.3%
Anhydrite
12.7%
Dolomite
18.2%
Calcite
66.8%

B

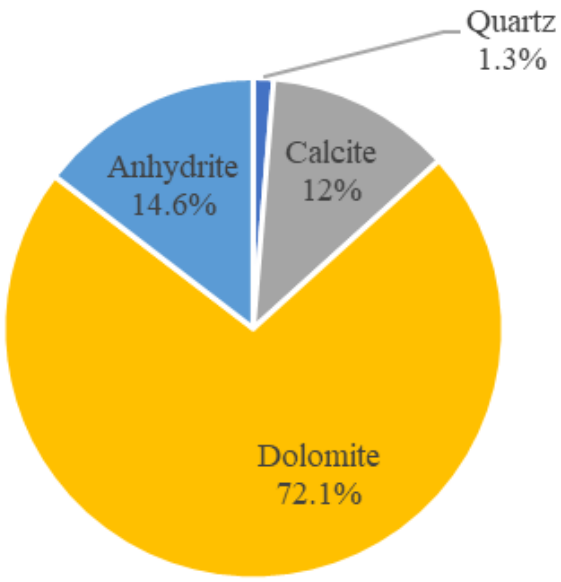
1F 4672
Quartz
1.3%
Anhydrite
14.6%
Calcite
12%
Dolomite
72.1%

C

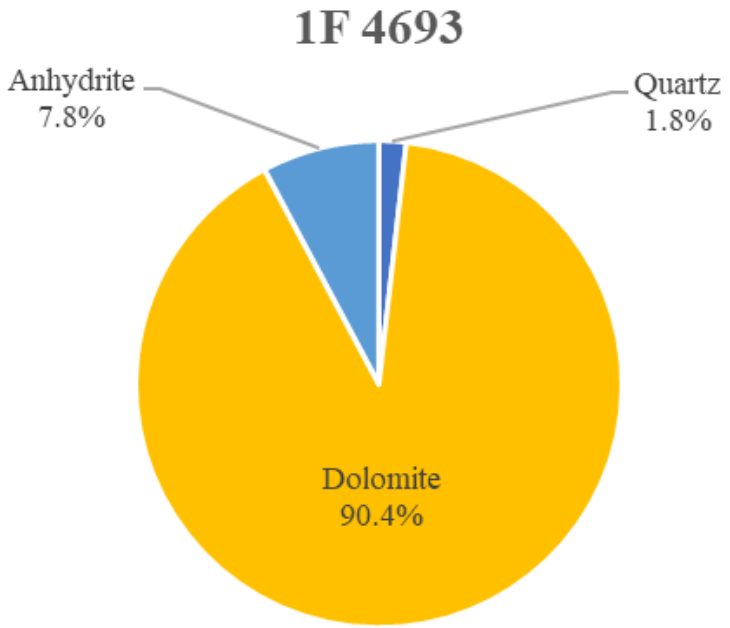
1F 4693
Anhydrite
7.8%
Quartz
1.8%
Dolomite
90.4%

D

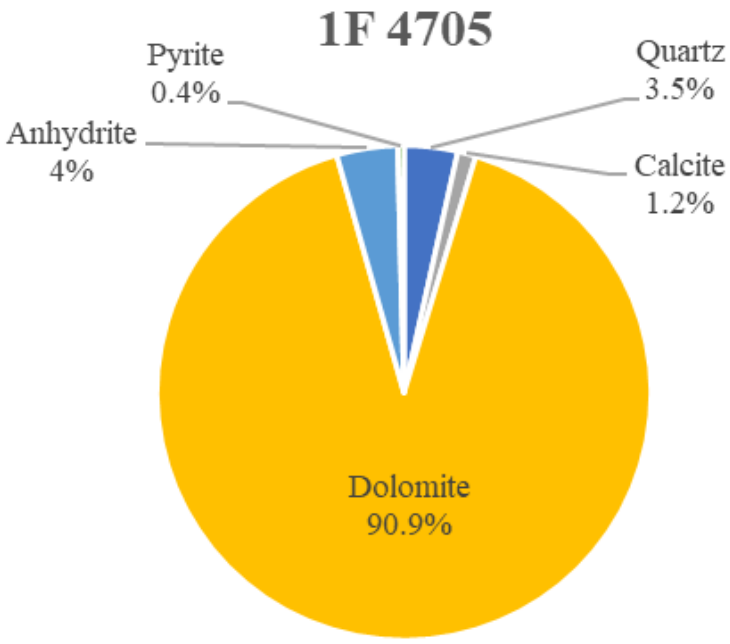
1F 4705
Pyrite
0.4%
Quartz
3.5%
Anhydrite
4%
Calcite
1.2%
Dolomite
90.9%

E

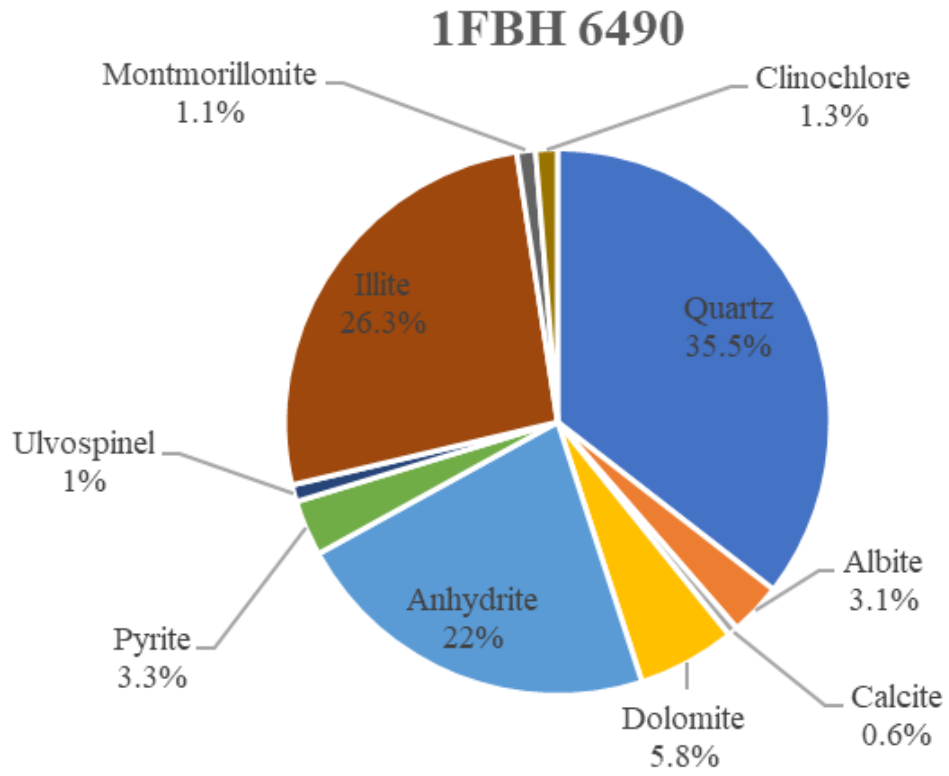
1FBH 6490
Montmorillonite 1.1%
Clinochlore 1.3%
Illite 26.3%
Quartz 35.5%
Ulvospinel 1%
Albite 3.1%
Anhydrite 22%
Pyrite 3.3%
Dolomite 5.8%
Calcite 0.6%

F

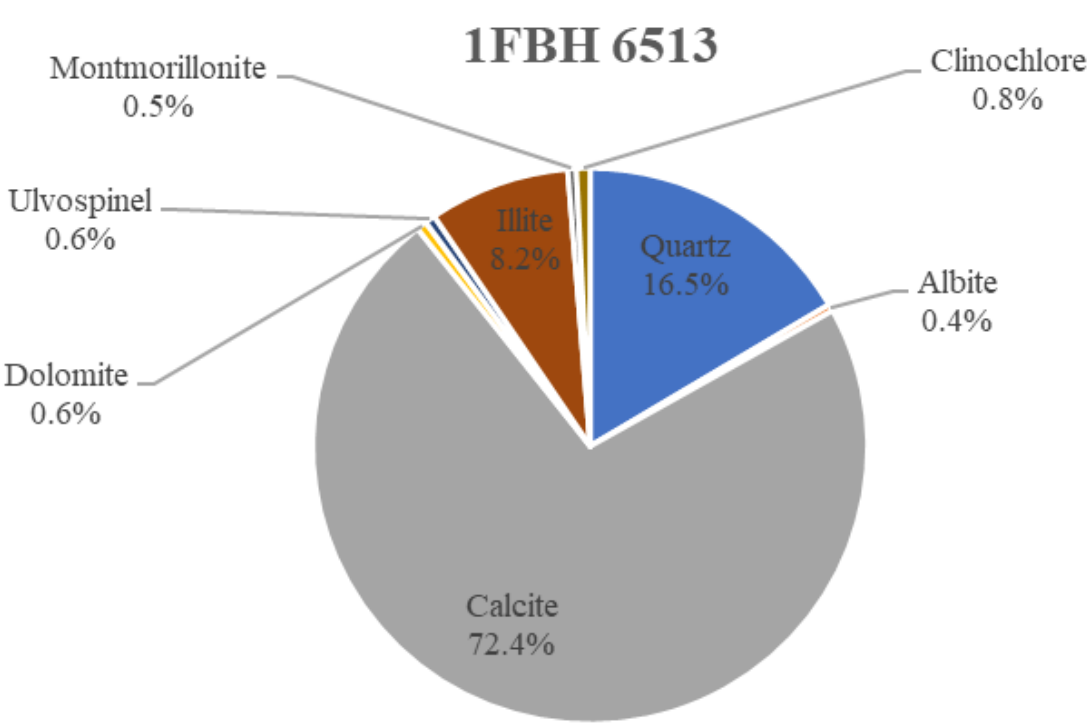
1FBH 6513
Montmorillonite 0.5%
Clinochlore 0.8%
Ulvospinel 0.6%
Illite 8.2%
Quartz 16.5%
Albite 0.4%
Dolomite 0.6%
Calcite 72.4%

G

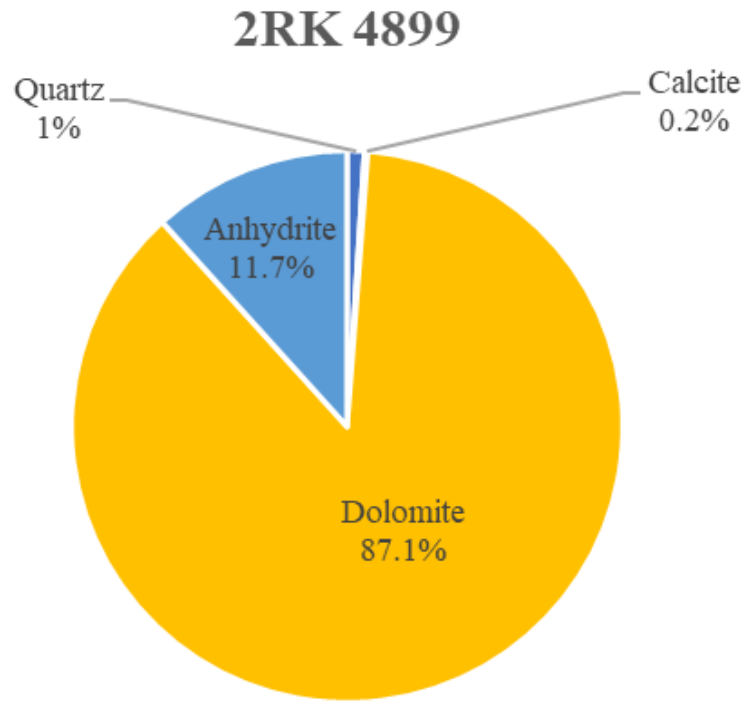
2RK 4899
Quartz
1%
Calcite
0.2%
Anhydrite
11.7%
Dolomite
87.1%

H

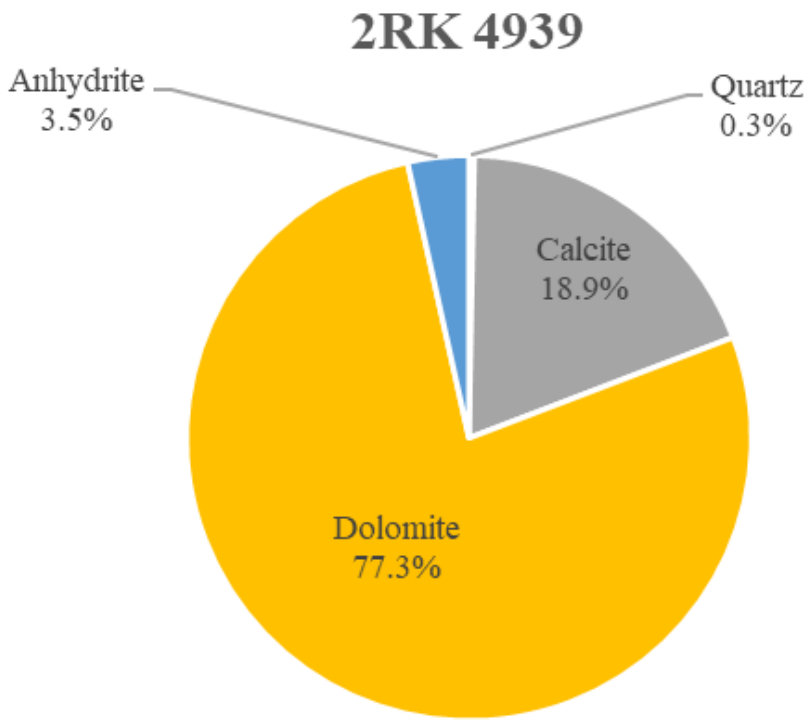
2RK 4939
Anhydrite
3.5%
Quartz
0.3%
Calcite
18.9%
Dolomite
77.3%

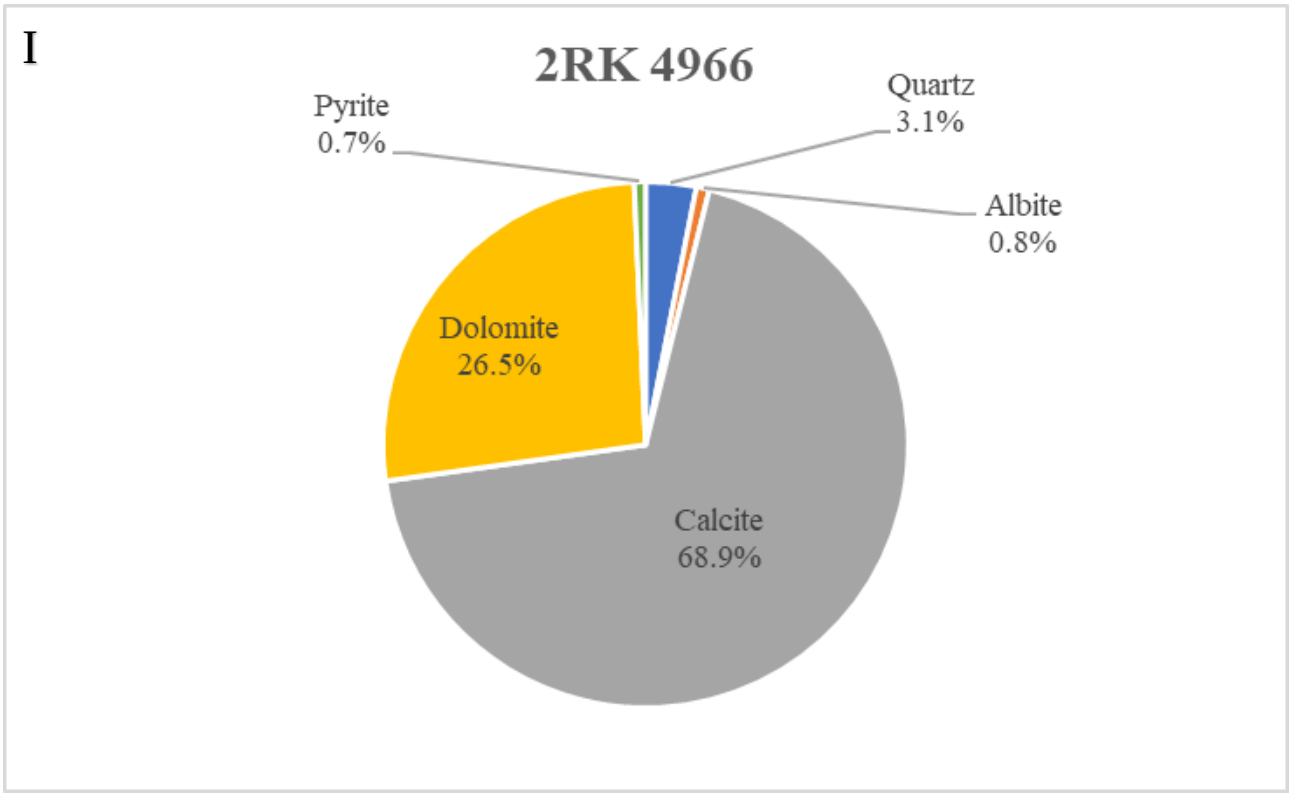

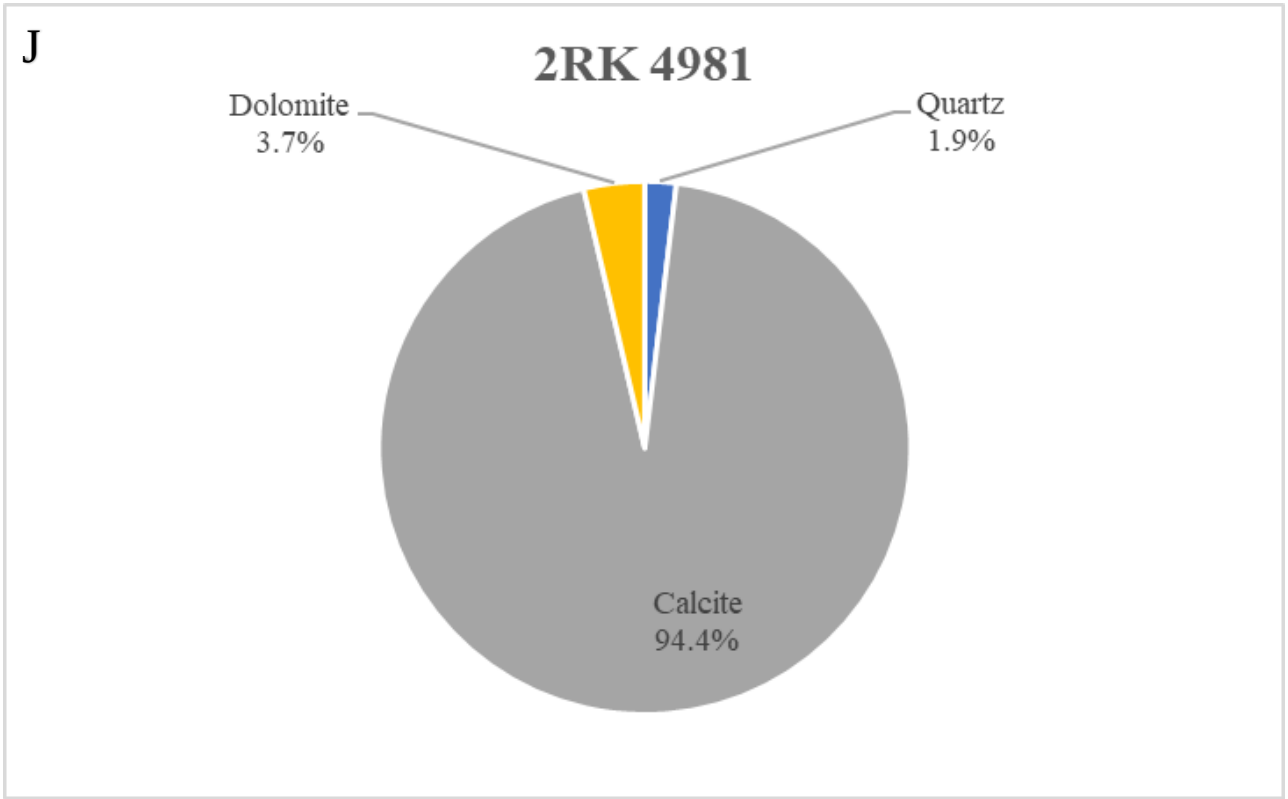

Figure 11: Mineral percentage charts A-J

4.2 TOC and Pyrolysis

TOC and pyrolysis data for all 10 samples are presented in Table 4. TOC percentages range from 0.08-4.76% with the carbonate-rich 1F and 2RK samples exhibiting the lower values (0.08-0.25%) and samples 1FBH 6490 and 6513 showing higher percentages of 4.76% and 1.56%, respectively. The pyrolysis analyses show that S1 values for the 1F and 2RK samples range from 0.05 to 0.14 mg HC/g with 1FBH 6490 and 6513 showing 1.37 and 0.27 mg HC/g, respectively. S2 values for the 1F and 2RK samples range from 0.05-0.30 mg HC/g with 1FBH 6490 and 6513 showing 4.52 and 0.71 mg HC/g respectively. Hydrogen and oxygen index values are plotted against each other to determine kerogen types (Figure 12). The majority of samples show Type III kerogen which is considered a gas prone type. 1FBH 6490 plotted to the left of the Type I kerogen line while IFBH 6513 is considered a Type II kerogen. Samples not shown within Figure 12 are Type III kerogen, but plotted so far to the right of the graph that including them would comprromise the graph quality. The S2 values were plotted against TOC to form a kerogen quality plot (Figure 13). All samples land within the Type III gas prone zone. These results are backed up by the S2/TOC versus depth plot (Figure 14) where all samples are clearly shown within the gas window.

Rock ID	TOC (wt %)	S1 (mg HC/g)	S2 (mg HC/g)	S3 (mg CO2/g)	Tmax (°C)	Calculated %Ro From Tmax	Hydrogen Index (S2x100/TOC)	Oxygen Index (S3x100/TOC)	S2/S3 Conc. (mg HC/mg CO2)	S1/TOC Norm. Oil Content	Production Index (S1/(S1+S2)
1F 4648	0.08	0.05	0.07	0.29	438	0.72	89	368	0	64	0.42
1F 4672	0.22	0.09	0.27	0.36	452	0.98	126	167	1	42	0.25
1F 4693	0.08	0.06	0.05	0.32	429	0.56	65	413	0	78	0.55
1F 4705	0.25	0.11	0.26	0.32	455	1.03	105	129	1	44	0.30
2RK 4899	0.13	0.07	0.06	0.47	428	0.54	46	362	0	54	0.54
2RK 4939	0.09	0.08	0.10	0.49	429	0.56	113	555	0	91	0.44
2RK 4966	0.12	0.07	0.09	0.20	435	0.67	74	164	0	57	0.44
2RK 4981	0.22	0.14	0.30	0.27	432	0.62	140	126	1	65	0.32
1FBH 6490	4.76	1.37	4.52	0.21	454	1.01	95	4	22	29	0.23
1FBH 6513	1.56	0.27	0.71	0.18	462	1.16	46	12	4	17	0.28

Table 4: TOC and pyrolysis data of Wolfcamp A samples

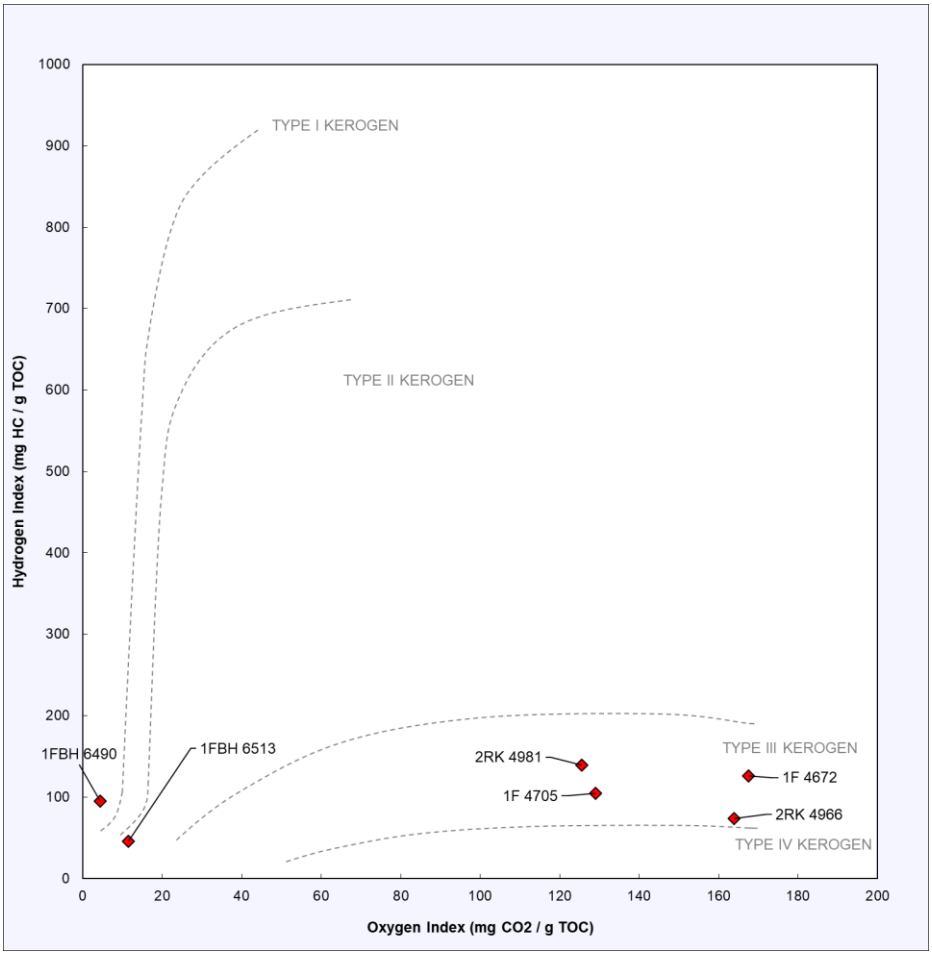

Figure 12: Pseudo van Krevlen plot for kerogen types.

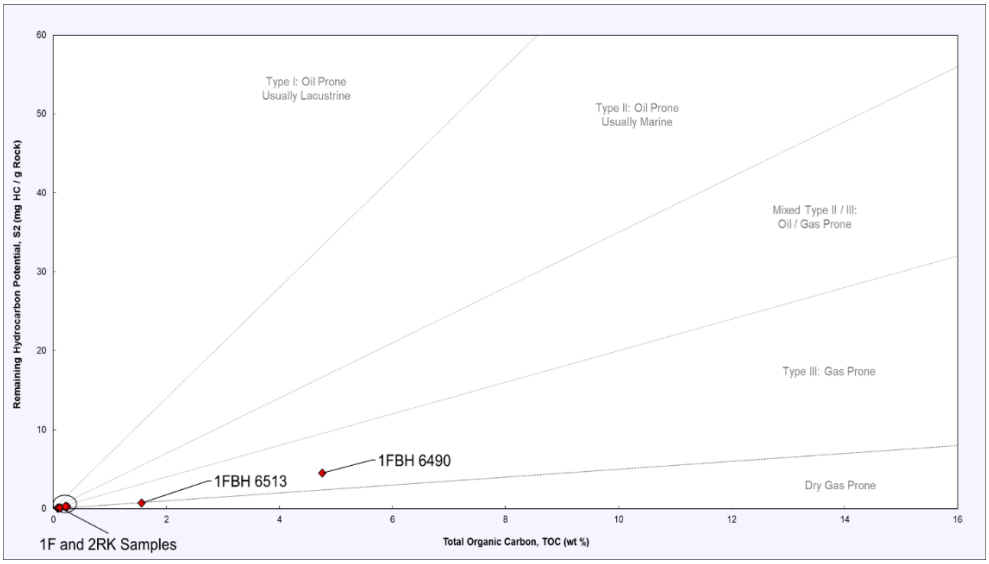

Figure 13: TOC vs. S2 kerogen quality plot.

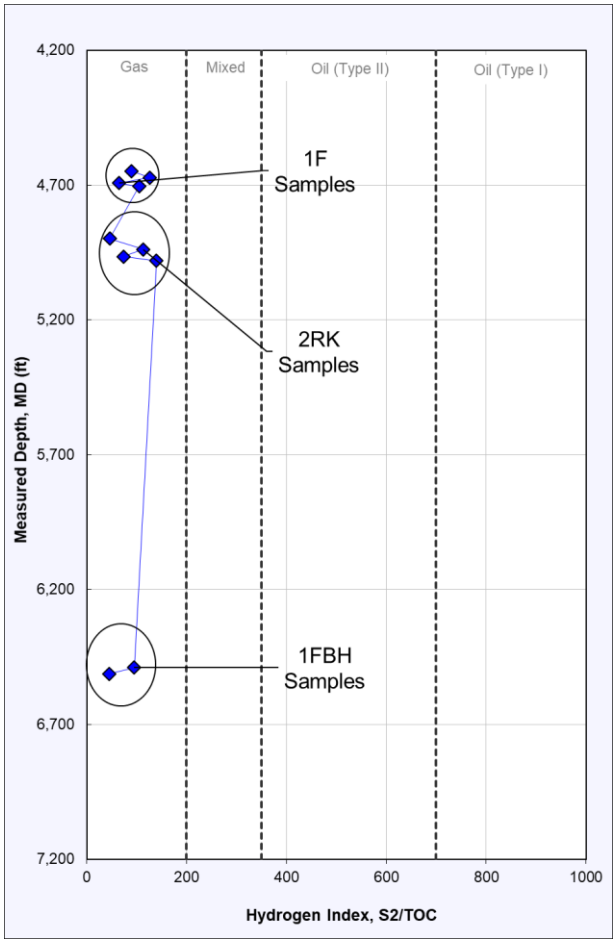

Figure 14: Kerogen quality vs. sample depth

4.3 Vacuum Saturation

Results from vacuum saturation tests are shown in Table 5. All 10 samples were tested to determine bulk density, grain density, and edge-accessible porosity. DI Water was used on irregular (large) size samples, plugs, and cubes. The irregular (large) size sample of 1FBH 6490 was not run because of its fragility, but plugs and cubes were tested. Two plugs that were cut parallel to the bedding plane were tested for the 1F 4648-4705 and 2RK 4899-4981 samples, and 3 plugs that were cut parallel to the bedding plane and 1 transverse to the bedding plane were tested for the 1FBH 6490-6513 samples. For all samples, three 1-cm cubes were tested with DI water. The averages were calculated for the plug and cube size runs with DI water, as shown in Table 4. For DT2 and THF fluids, one 1-cm cube was tested. The edge-accessible porosity for DIW ranges from 0.249-9.365% for large irregularly-sized core samples, from 0.757-10.0% for plugs, and from 0.869-9.80% for cubes. DT2 porosity ranges from 1.60-10.4%, and THF porosity ranges from 0.648-9.94%. The wide range of porosity percentages can be attributed to 2 samples, 1F 4705 and 2RK 4939 which consistently show around 9%. For most samples a trend can be seen where the edge-accessible porosity increases as sample size decreases. Another trend present is the increase in porosity when using DT2 as compared to DIW fluids. The only sample that did not show an increase in this situation was 2RK 4939. No real trend can be seen with THF, the assumption here is that it is due to its high evaporation rate from the fluid-saturated samples, with its measured porosity denoted as a low bound.

Sample ID		DI Water			DT2			THF		
	Size	Bulk Density (g/cm3)	Grain Density (g/cm3)	Porosity (%)	Bulk Density (g/cm3)	Grain Density (g/cm3)	Porosity (%)	Bulk Density (g/cm3)	Grain Density (g/cm3)	Porosity (%)
1F-4648	Half Core	2.706	2.725	0.678						
	Plug	2.705	2.741	1.303						
	1 cm Cube	2.716	2.75	1.23	2.800	2.856	1.967	2.651	2.689	1.436
1F-4672	Half Core	2.726	2.753	0.965						
	Plug	2.797	2.836	1.399						
	1 cm Cube	2.774	2.84	2.309	2.812	2.880	2.373	2.842	2.882	1.386
1F-4693	Half Core	2.648	2.719	2.607						
	Plug	2.731	2.881	5.201						
	1 cm Cube	2.727	2.890	5.623	2.781	2.949	5.705	2.724	2.855	4.575
1F-4705	Half Core	2.470	2.726	9.365						
	Plug	2.540	2.824	10.048						
	1 cm Cube	2.566	2.844	9.799	2.608	2.912	10.436	2.550	2.831	9.937
1FBH-6490	Full Core	N/A	N/A	N/A						
	Plug	2.449	2.533	3.315						
	1 cm Cube	2.493	2.579	3.37	2.495	2.609	4.377	2.522	2.659	5.155
1FBH-6513	Full Core	2.635	2.666	1.134						
	Plug	2.639	2.695	2.107						
	1 cm Cube	2.608	2.676	2.531	2.638	2.725	3.185	2.576	2.642	2.500
2RK-4899	Half Core	2.819	2.848	0.647						
	Plug	2.830	2.855	0.890						
	1 cm Cube	2.823	2.856	0.869	2.881	2.928	1.599	2.804	2.822	0.648
2RK-4939	Half Core	2.553	2.773	7.391						
	Plug	2.602	2.856	8.859						
	1 cm Cube	2.59	2.795	8.673	2.721	2.886	5.724	2.566	2.817	8.916
2RK-4966	Half Core	2.709	2.715	0.249						
	Plug	2.737	2.761	0.900						
	1 cm Cube	2.702	2.729	0.985	2.749	2.802	1.893	2.675	2.696	0.782
2RK-4981	Half Core	2.680	2.694	0.511						
	Plug	2.693	2.713	0.757						
	1 cm Cube	2.687	2.723	1.317	2.722	2.780	2.078	2.660	2.706	1.675

Table 5: Result Compilation from Vacuum Saturation

4.4 Mercury Intrusion Porosimetry

Mercury Intrusion Porosimetry (MIP) is used to determine pore-throat size distribution within a sample, and is considered one of the most important and cost-effective testing

procedures for pore structure characterization. The method preformed for this process was shown by Gao and Hu (2013) and involves picking inflection points which are indicators of maximum intrusion pressures among two connected pore networks. An example can be seen in Figure 15, these peaks indicate that mercury has intruded into a new pore network. Seven of 10 samples were subjected to MIP testing, these include 1F 4648, 1F 4693, 1F 4705 1FBH 6490, 2RK 4899, 2RK 4939, and 2RK 4981.

Pore type and pore-throat diameter qualitatively share a relationship with one another. Pores with a diameter between 0.0028-0.005 μm are considered to be inter-clay platelet pores, pores with a diameter between 0.005-0.01 μm as organic pores, pores with diameters between 0.01-0.05 μm and 0.05-1 μm as intergranular pores, and pores with a diameter between 1-1100 μm are micro-fractures. Pore-throat size distributions of all samples are presented in Table 6 and a graphical representation is shown as Figure 16. All samples within this study show intergranular pores as their dominant pore types. 1FBH 6490 and 2RK 4939 are the only samples to exhibit inter-clay platelet pore types at 21.14 and 0.74% of total pore volumes, respectively. Samples 1F 4648, 1FBH 6490, 2RK 4899, and 2RK 4939 are the only ones to show organic pores and come in at 4.26%, 22.33%, 0.98%, and 0.43%, respectively. All samples contain the remaining pore types.

Along with pore throat size distribution, MIP can quantify many other properties such as porosity, permeability, tortuosity, bulk density, apparent (skeletal) density, total pore area, and pore volume. The results for all samples can be seen in Table 7. Porosity for the 1F samples ranges from 1.00-9.74%, and total pore area ranges from 0.70-0.93 m^2/g. For sample 1FBH 6490, the porosity is 2.68% and the total pore area is 5.08 m^2/g. Porosity for the 2RK samples ranges from 0.448-7.66%, and the total pore area ranges from 0.14-2.53 m^2/g.

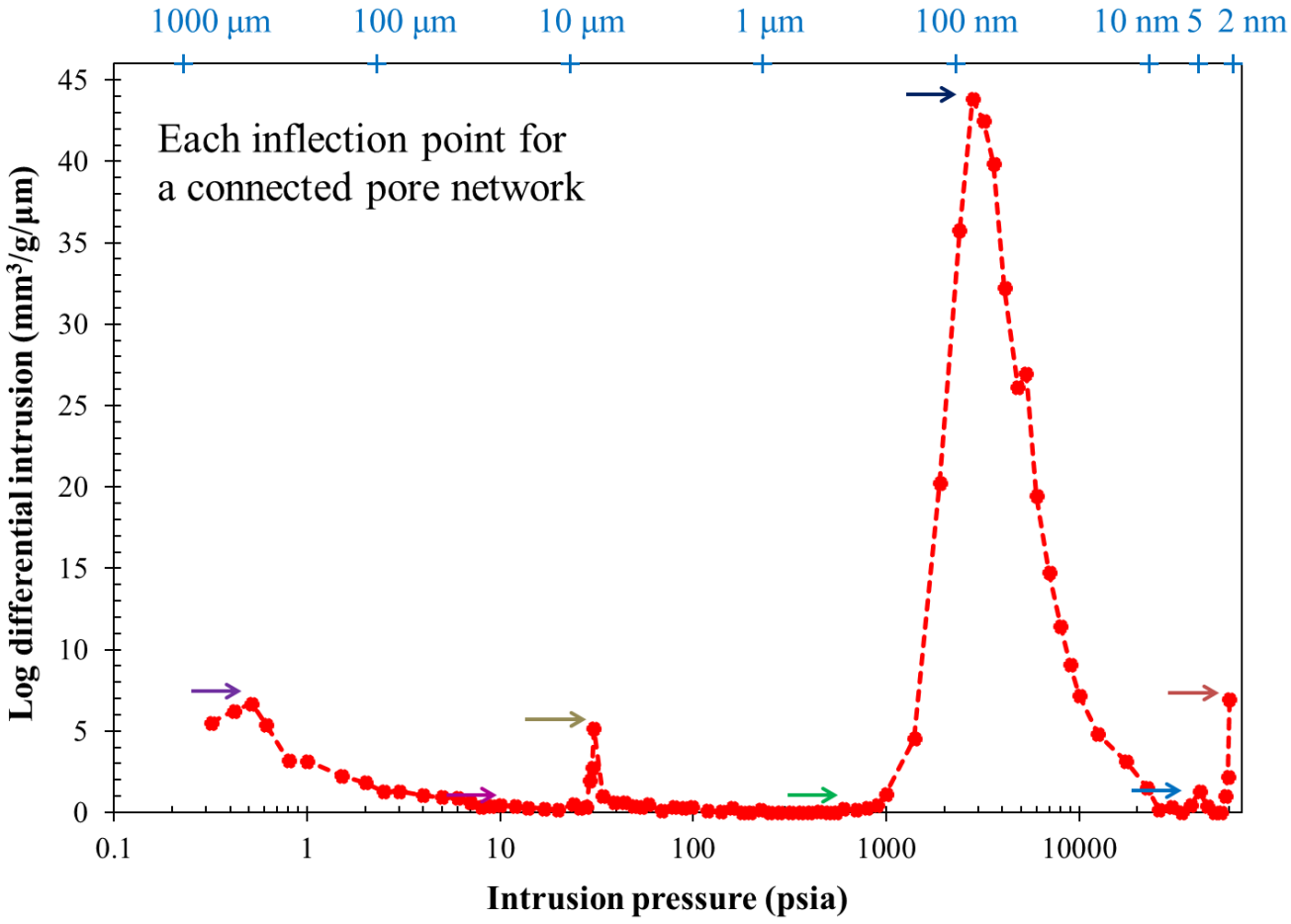

Figure 15: MIP plot of 2RK 4939 showing inflection points (arrows); the 2nd X-axis indicated the pore-throat sizes corresponding to the intrusion pressure.

Sample ID	0.0028-0.005 µm	0.005-0.01 µm	0.01-0.05 µm	0.05-0.1 µm	0.1-1 µm	1-10 µm	10-50 µm	10-100 µm	100-1100 µm
1F 4648	0.00	4.26	75.40	5.63	2.42	3.16	9.14		
1F 4693	0.00	0.00	11.78	20.13	61.07	4.44	2.58		
1F 4705	0.00	0.00	2.81	3.47	81.23	4.09		1.46	6.96
1FBH 6490	21.14	22.33	21.16	4.15	9.77	18.38	3.07		
2RK 4899	0.00	0.98	29.92	13.22	14.15	17.45	24.29		
2RK 4939	0.74	0.43	19.66	37.27	24.01	1.48		2.06	14.35
2RK 4981	0.00	0.00	60.00	20.11	8.54	6.54	4.81		

Table 6: MIP results for the distribution (%) of specific regions of pore-throat diameters

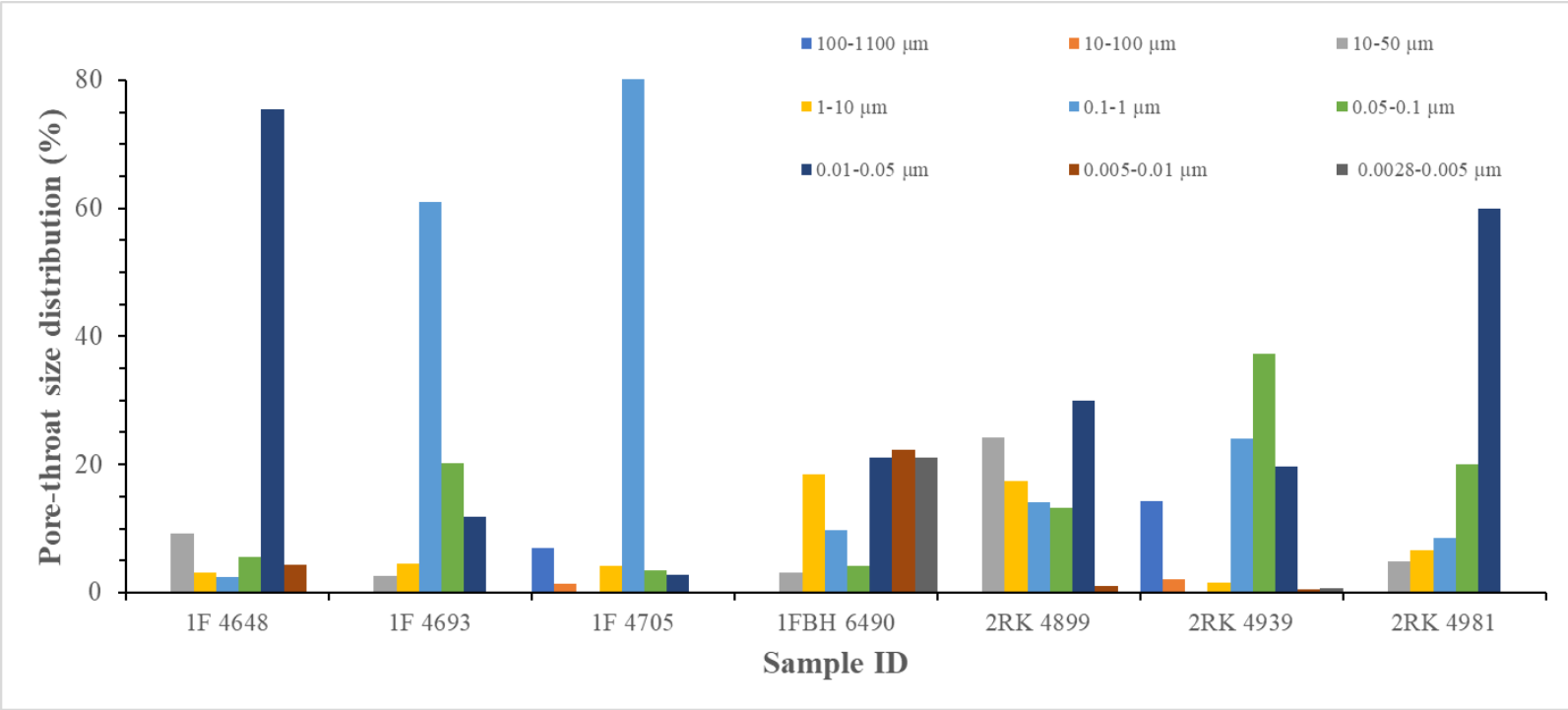

Figure 16: Pore-throat size distribution comparison

Sample ID	Bulk density (g/cm^3)	Apparent (skeletal) density (g/cm^3)	Total pore area (m^2/g)	Porosity (%)	Pore-throat region	Pore volume	Permeability (mD)	Tortuosity (D0/De)
1F 4648	2.67	2.70	0.81	1.0044	10-50 µm	0.091	1.944E+00	2.66
					1-10 µm	0.032	4.170E-01	5.74
					0.1-1 µm	0.024	3.421E-04	200.34
					10-100 nm	0.810	2.163E-05	796.64
					5-10 nm	0.000	0	0
					2.8-5 nm	0.000	0	0
1F 4693	2.67	2.81	0.93	4.8847	1-50 µm	0.026	3.297E+00	2.69
					0.1-1 µm	0.044	1.275E-01	13.68
					10-100 nm	0.611	5.676E-03	64.82
					5-10 nm	0.319	1.492E-04	400
					2.8-5 nm	0.000	0	0
1F 4705	2.40	2.66	0.70	9.7445	100-1100 µm	0.000	4.560E+02	6.50
					10-100 µm	0.041	5.273E+01	19.10
					1-10 µm	0.812	2.614E+00	85.81
					0.1-1 µm	0.063	1.459E-01	363.18
					10-100 nm	0.000	6.998E-04	5244.03
					5-10 nm	0.000	0	0
					2.8-5 nm	0.000	0	0
1FBH 6490	2.46	2.52	5.08	2.6815	10-50 µm	0.031	8.178E-01	3.82
					1-10 µm	0.184	7.923E-01	3.88
					0.1-1 µm	0.098	5.034E-02	15.38
					10-100 nm	0.253	3.835E-06	1762.25
					5-10 nm	0.223	2.267E-06	2292.38
					2.8-5 nm	0.211	2.406E-06	2224.79
2RK 4899	2.74	2.76	0.14	0.4477	10-50 µm	0.243	2.546E+00	2.77
					1-10 µm	0.175	3.967E-01	7.02
					0.1-1 µm	0.141	1.690E-03	107.55
					10-100 nm	0.431	1.257E-05	1247.36
					5-10 nm	0.000	0	0
					2.8-5 nm	0.000	0	0
2RK 4939	2.55	2.76	2.53	7.6611	100-1100 µm	0.143	1.1264E+04	2.04
					10-100 µm	0.021	3.1006E+01	38.94
					1-10 µm	0.015	3.5597E+00	114.94
					0.1-1 µm	0.240	9.0076E-04	7255.39
					10-100 nm	0.569	1.9956E-03	4854.34
					5-10 nm	0.004	3.9612E-06	108957.04
					2.8-5 nm	0.007	6.869E-06	82743.6
2RK 4981	2.68	2.70	0.24	0.4941	10-50 µm	0.048	1.292E-01	4.71
					1-10 µm	0.065	3.690E-02	8.81
					0.1-1 µm	0.085	3.999E-04	84.66
					10-100 nm	0.801	2.036E-05	375.20
					5-10 nm	0.000	0	0
					2.8-5 nm	0.000	0	0

Table 7: Summary of MICP results

4.5 Contact Angle and Wettability

Contact angle measurements are used to determine the wettability of a sample to a fluid on a polished surface. Contact angle measurements were taken on 8 of 10 samples using five different fluids. These fluids include DIW, API brine, 20% IPA, 20% THF, and DT2. Values for contact angle using DIW, API Brine, 20% IPA and THF were taken at 30 seconds after the droplet of fluid touches the sample surface, but DT2 measurements were taken in less than one second due to its tendency to rapidly spread across the sample's surface and the machine's 3 degree detection limit. Images of measurement methods for 2RK 4939 can be seen in Figure 17 and the contact angle results are presented in Table 8. All samples show a mostly oil-wet, with partially water-wet, wettability.

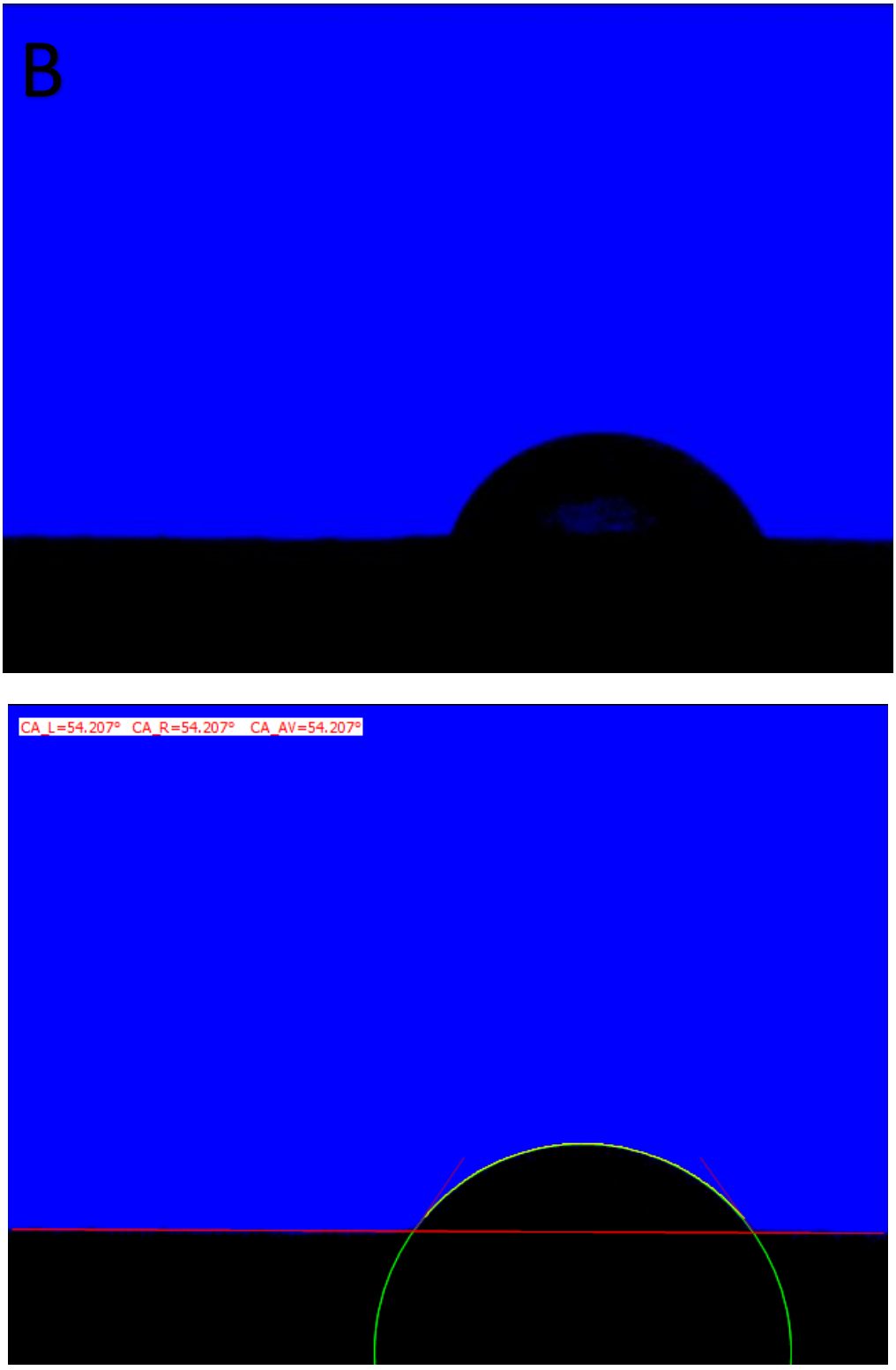

Figure 17 (A-C): A) before droplet is released, B) as droplet touches sample surface, C) 30 sec after droplet touches sample surface

Sample ID	After 30 sec				Within 1 sec
	DI Water	API Brine	20% IPA	20% THF	DT2
1F 4648	44.16	81.44	27.44	39.19	9.32 to 3.0
1F 4672	46.02	65.68	N/A	50.27	9.52 to 3.0
1F 4693	57.52	41.14	N/A	54.66	4.59 to 3.0
1F 4705	42.58	63.95	N/A	16.30	10.59 to 3.0
1FBH 6490	32.50	34.36	N/A	30.07	5.85 to 3.0
2RK 4899	41.32	54.75	44.62	62.66	8.84 to 3.0
2RK 4939	54.21	62.14	N/A	46.22	8.18 to 3.0
2RK 4981	70.00	42.73	N/A	43.12	16.13 to 3.0

Table 8: Contact angle measurements in degrees

4.6 Spontaneous Imbibition

All 10 samples were subjected to imbibition testing using DIW and DT2, but DT2 results for 2RK 4966 were compromised and I was unable to re-test the sample. The imbibition results generally show 2-3 slopes, but occasionally a 4th slope is present. These slopes represent certain stages of fluid uptake. The first Stage, or associated Type I slope, occurs within the first few seconds of the experiment and is related to the settling behavior caused by the sample touching the fluid surface. The slope during Stage one typically reads from 2 to 4. Stage two, or Type II slope, relates to the initial fluid uptake of the sample's edge and through microfractures/laminations. This slope typically occurs within minutes and reads around 0.75. Stage three, or Type III slope, is the connectivity slope of, and relates to the fluid migration into and through, the sample matrix. This stage shows if the pore networks of the sample is either well- or poorly-connected. A value at 0.5 or above, in a log imbibed mass vs. log imbibition time, indicates a well-connected space, around 0.26 indicates a poor connection, and anything in between is considered intermediate connectivity (Hu et al., 2012). Stage four indicates that the

fluid has reached the top of the sample (Hu et al., 2001); this is especially applicable for the DT2 runs because of its excellent wettability and fast imbibition.

DIW imbibition tests were ran for 24 hours and DT2 for 6 hours. The connectivity slope values along with the connectivity classification can be seen in Table 9 with graphical images presented in Figures 18-27. The slope for samples 1F 4648-4705 using DIW ranges from 0.236-0.375 and from 0.503-0.875 using DT2. The slope for samples 1FBH 6490-6513 using DIW are 0.628 and 0.300, respectively. For DT2 they are 0.848 and 0.330, respectively. The slope for sample 2RK 4899-4981 using DIW range from 0.277-0.456 and from 0.290-0.652 using DT2. Overall, the samples show an intermediate connectivity slope for water and a high connectivity slope for DT2. Two exceptions come with using DIW, for 1F 4693 the connectivity is low (0.256) and for 1FBH 6490 the connectivity is high (0.628). In addition, two exceptions occurred with using DT2, for 1FBH 6513 and 2RK 4939 the connectivity is intermediate (0.330 and 0.290, respectively).

Sample ID	DI Water	Connectivity Classification	DT2	Connectivity Classification
1F 4648	0.274	Intermediate	0.875	High
1F 4672	0.375	Intermediate	0.503	High
1F 4693	0.236	Low	0.700	High
1F 4705	0.330	Intermediate	0.531	High
1FBH 6490	0.628	High	0.848	High
1FBH 6513	0.300	Intermediate	0.330	Intermediate
2RK 4899	0.287	Intermediate	0.652	High
2RK 4939	0.456	Intermediate	0.290	Intermediate
2RK 4966	0.365	Intermediate	N/A	N/A
2RK 4981	0.277	Intermediate	0.512	High

Table 9: Connectivity slope results for the 3rd Stage

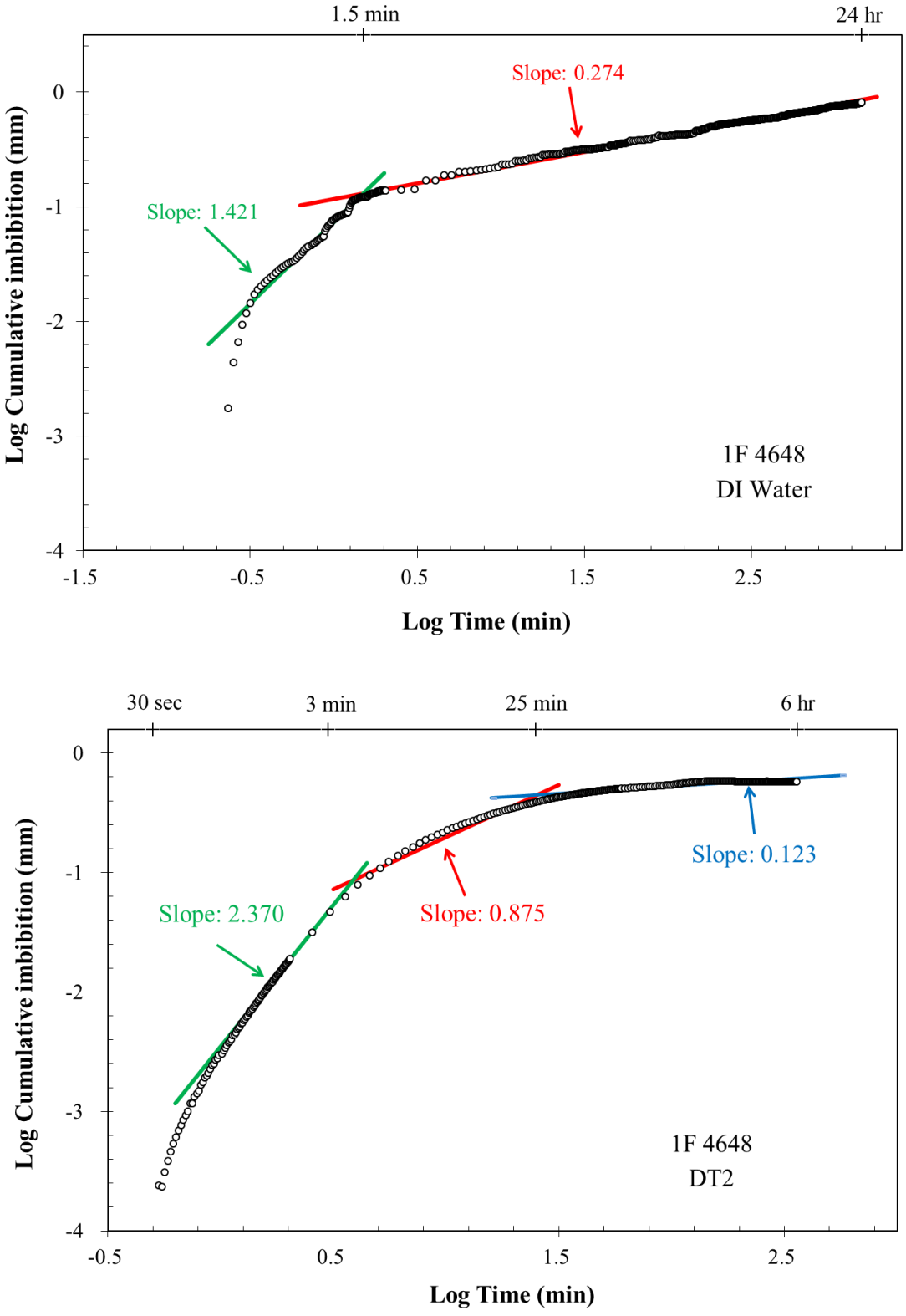

Figure 18: 1F 4648 Imbibition graph using DIW (top) and DT2 (bottom)

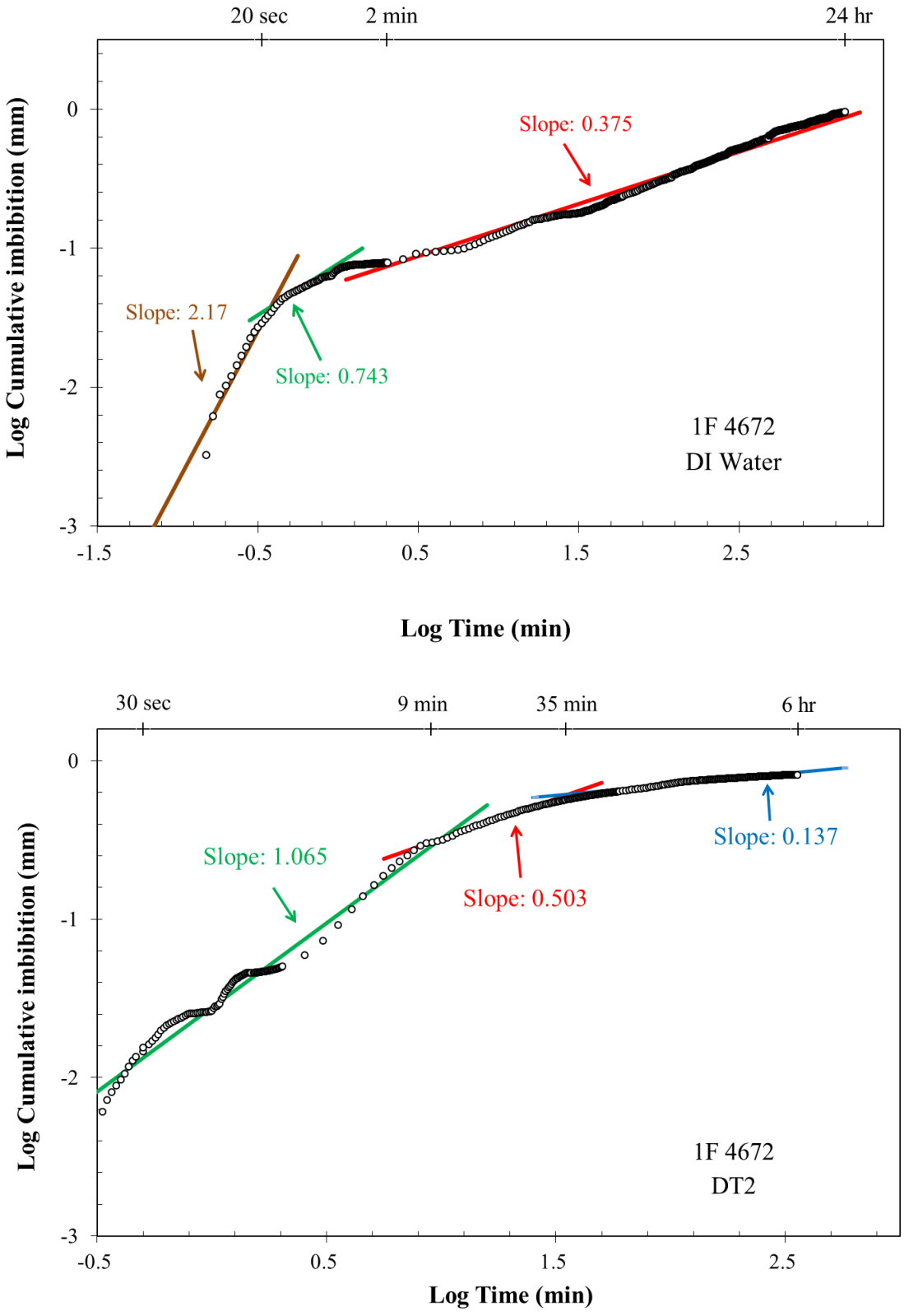

Figure 19: 1F 4672 Imbibition graph using DIW (top) and DT2 (bottom)

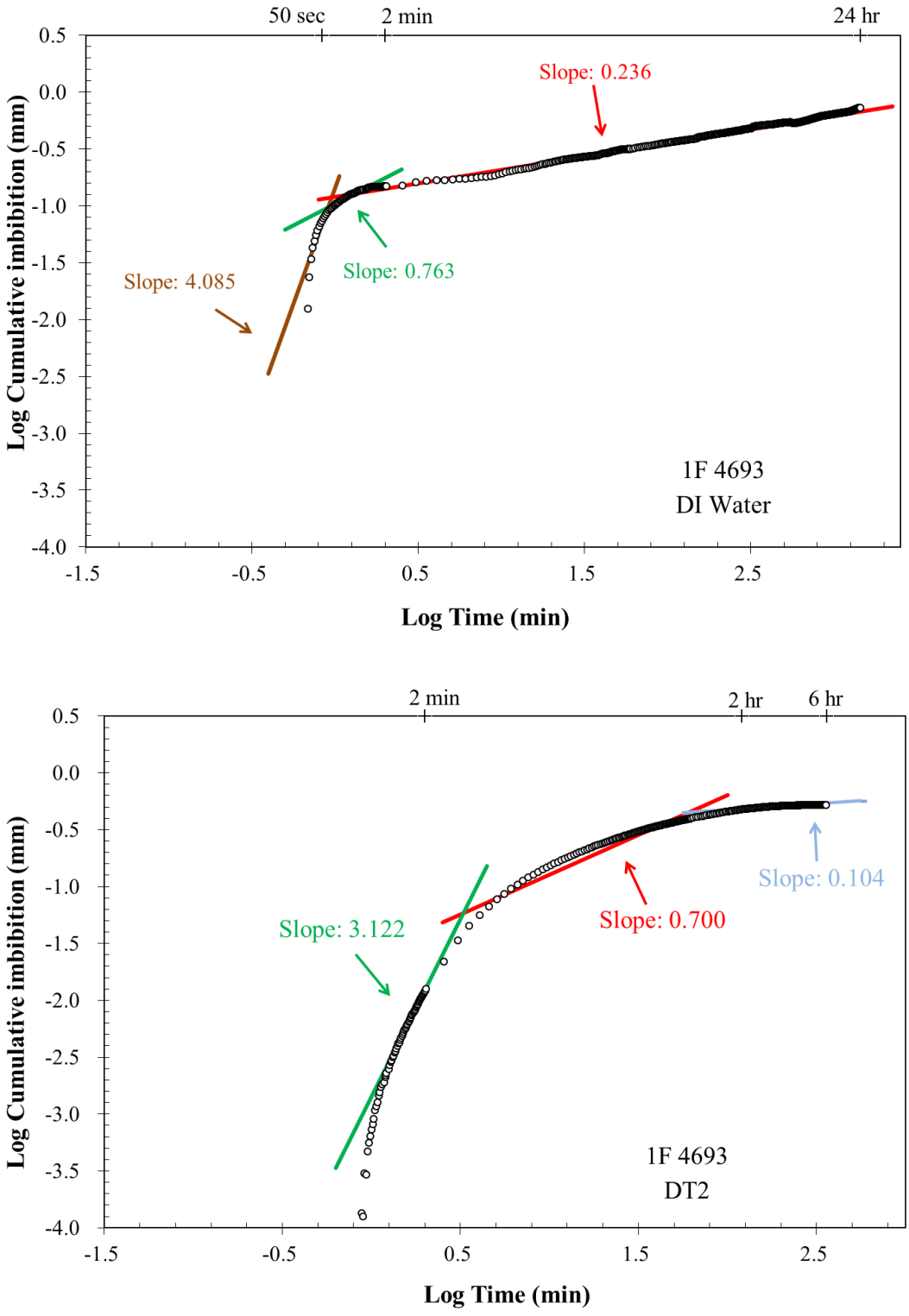

Figure 20: 1F 4693 Imbibition graph using DIW (top) and DT2 (bottom)

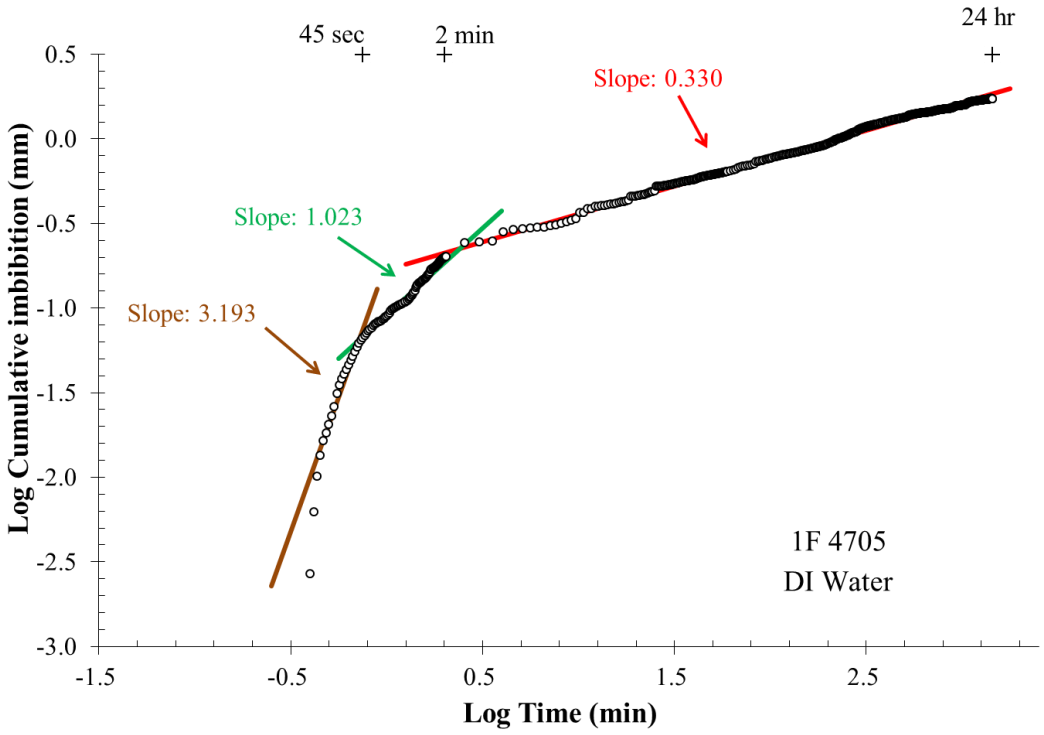

Figure 21: 1F 4705 Imbibition graph using DIW (top) and DT2 (bottom)

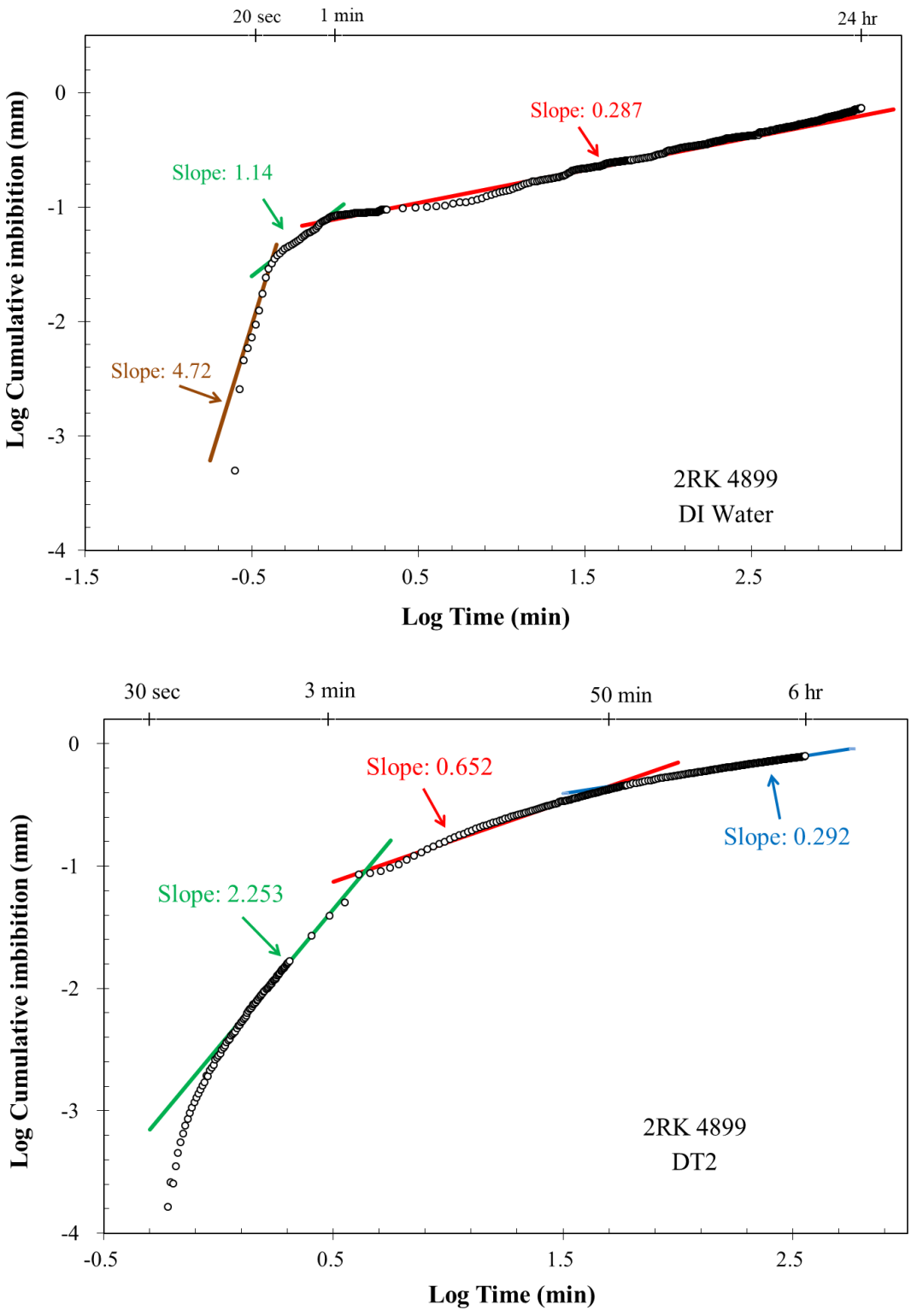

Figure 22: 2RK 4899 Imbibition graph using DIW (top) and DT2 (bottom)

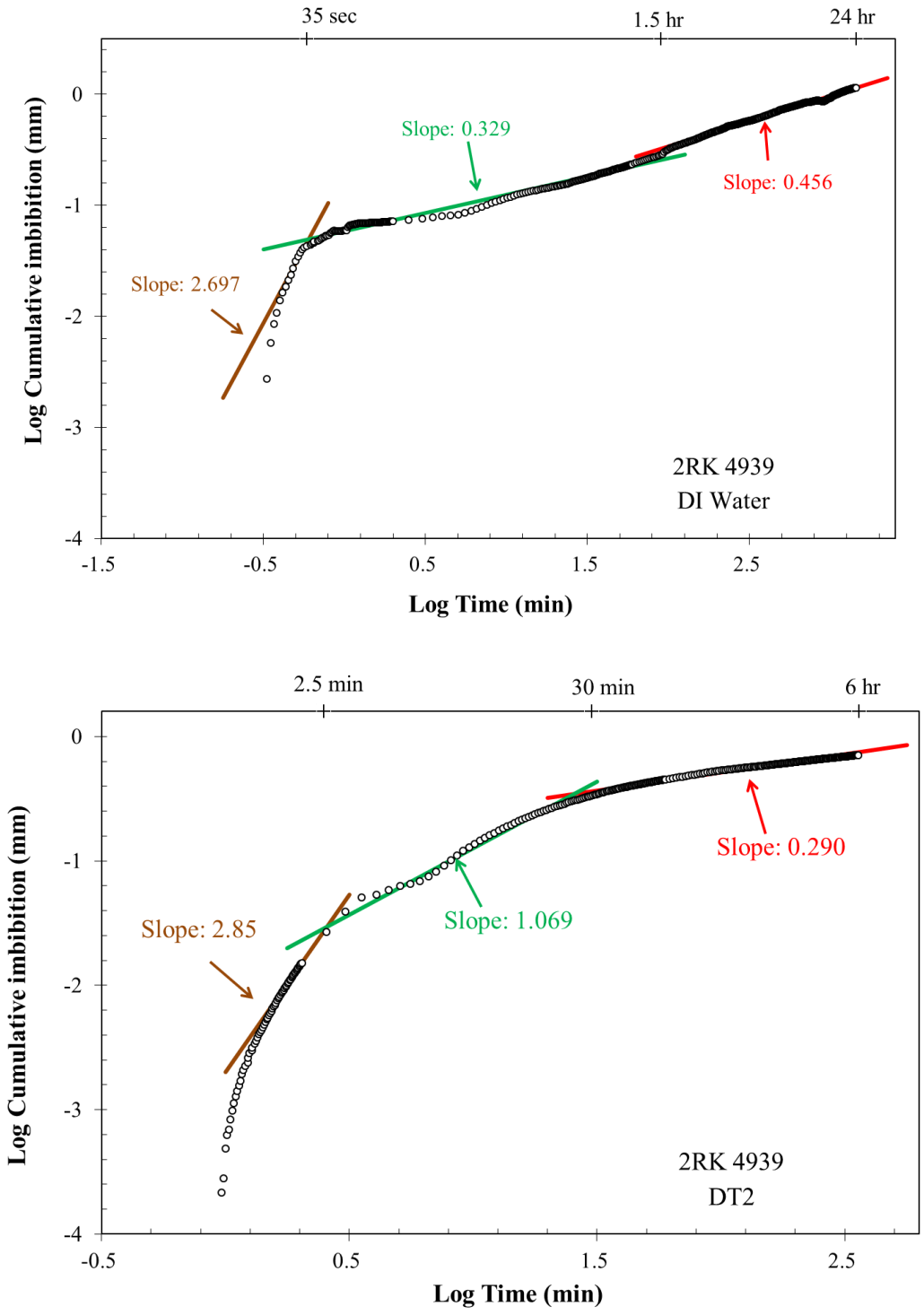

Figure 23: 2RK 4939 Imbibition graph using DIW (top) and DT2 (bottom)

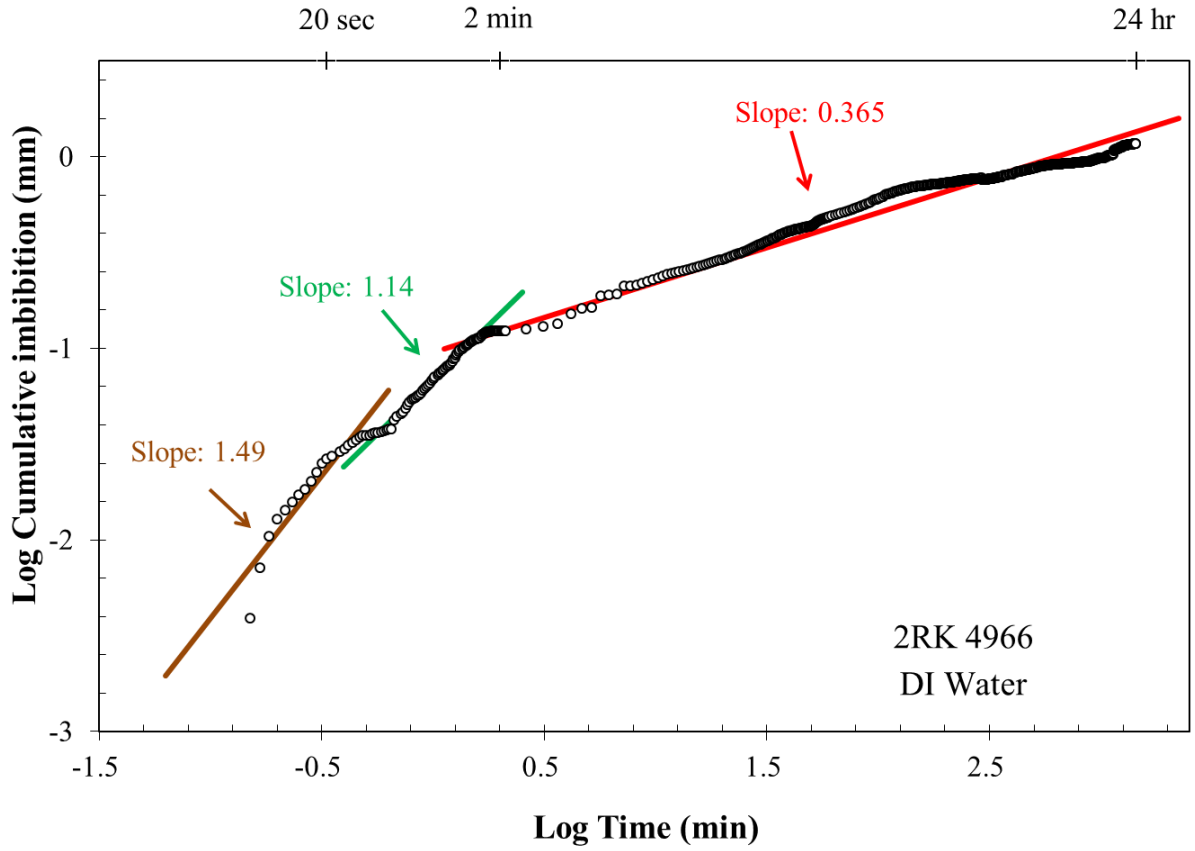

Figure 24: 2RK 4966 imbibition graph using DIW

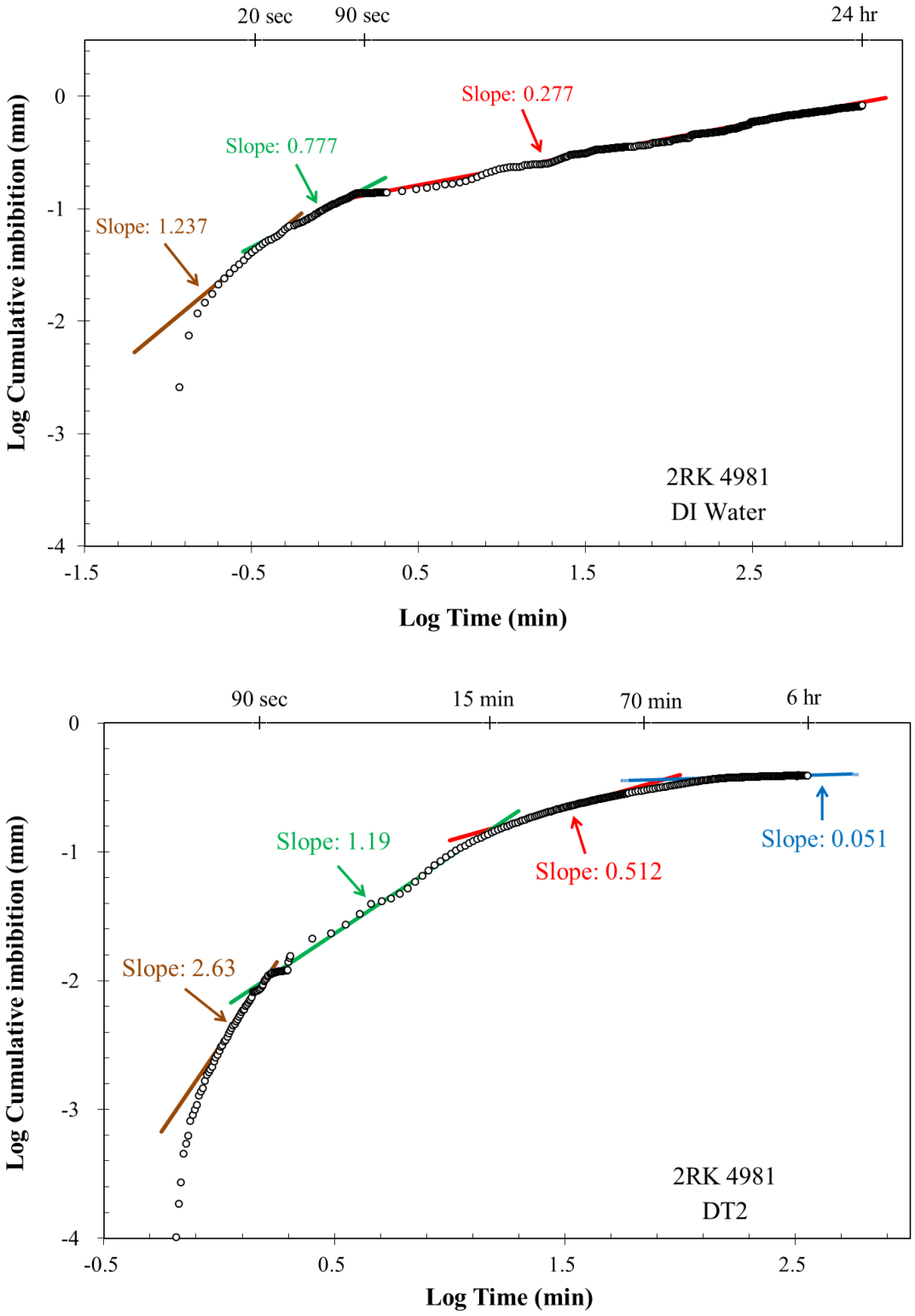

Figure 25: 2RK 4981 Imbibition graph using DIW (top) and DT2 (bottom)

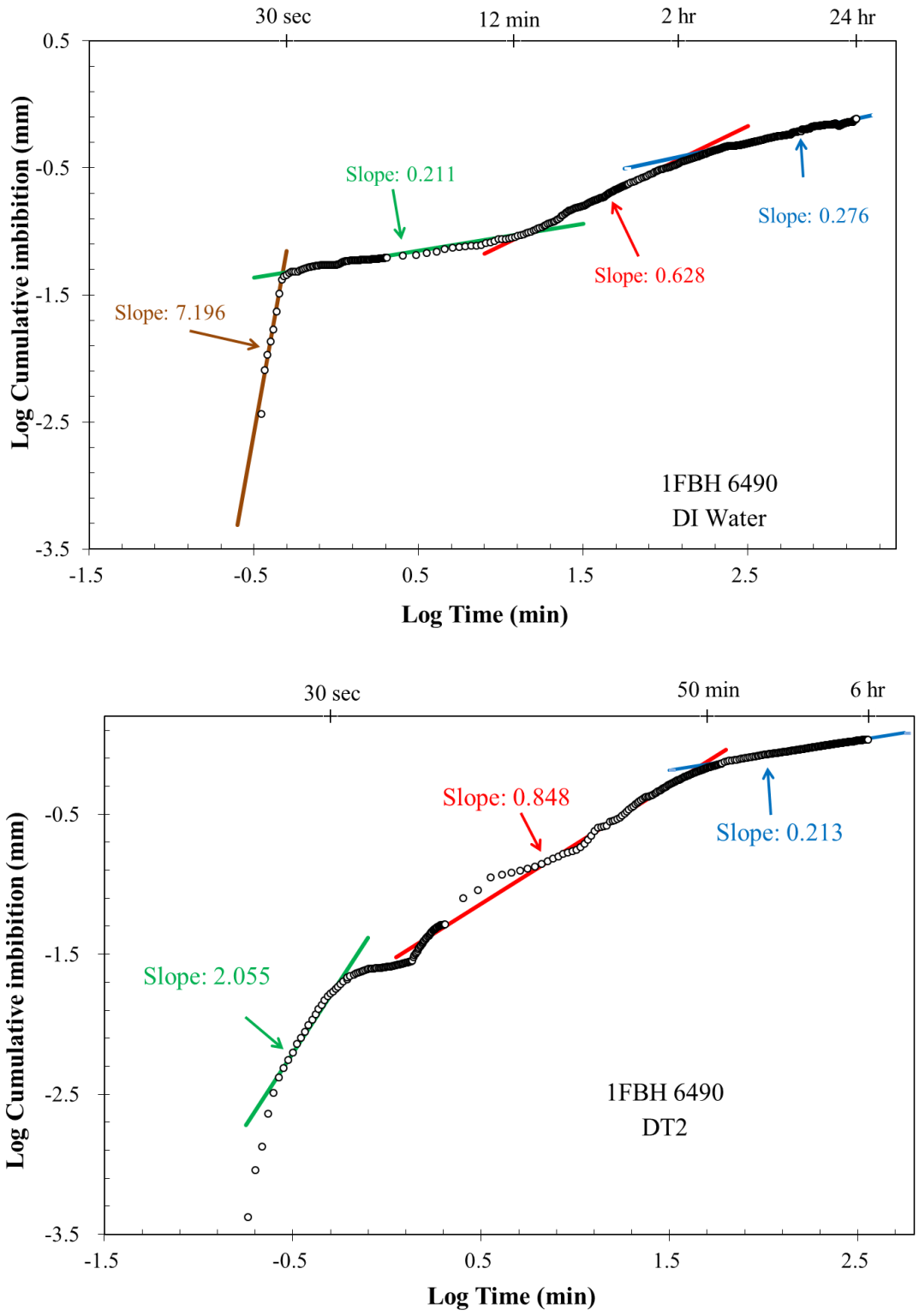

Figure 26: 1FBH 6490 Imbibition graph using DIW (top) and DT2 (bottom)

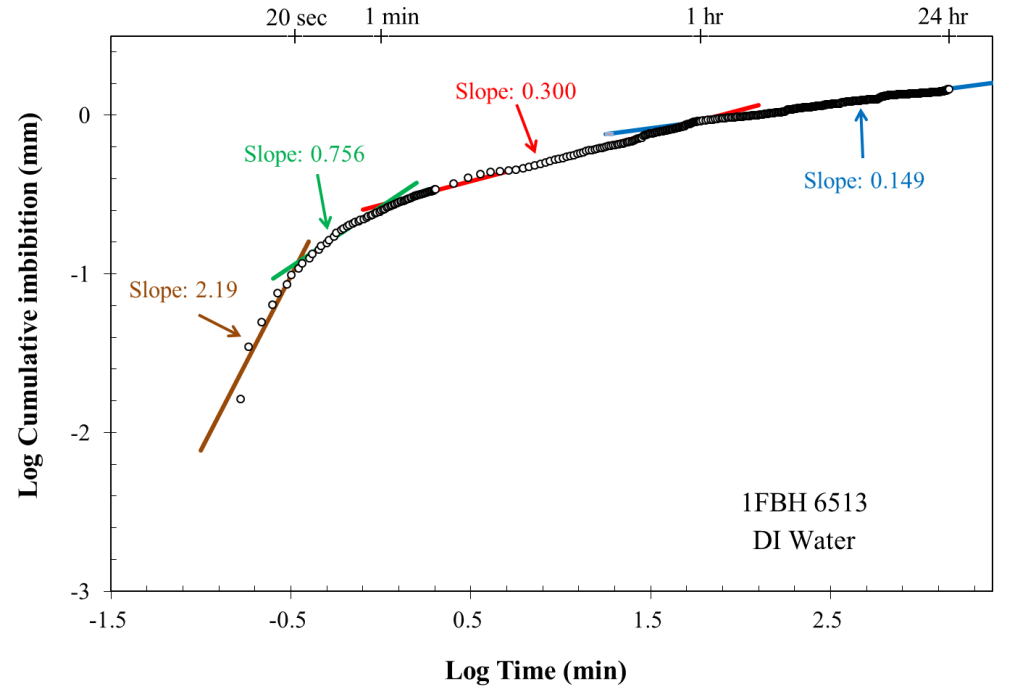

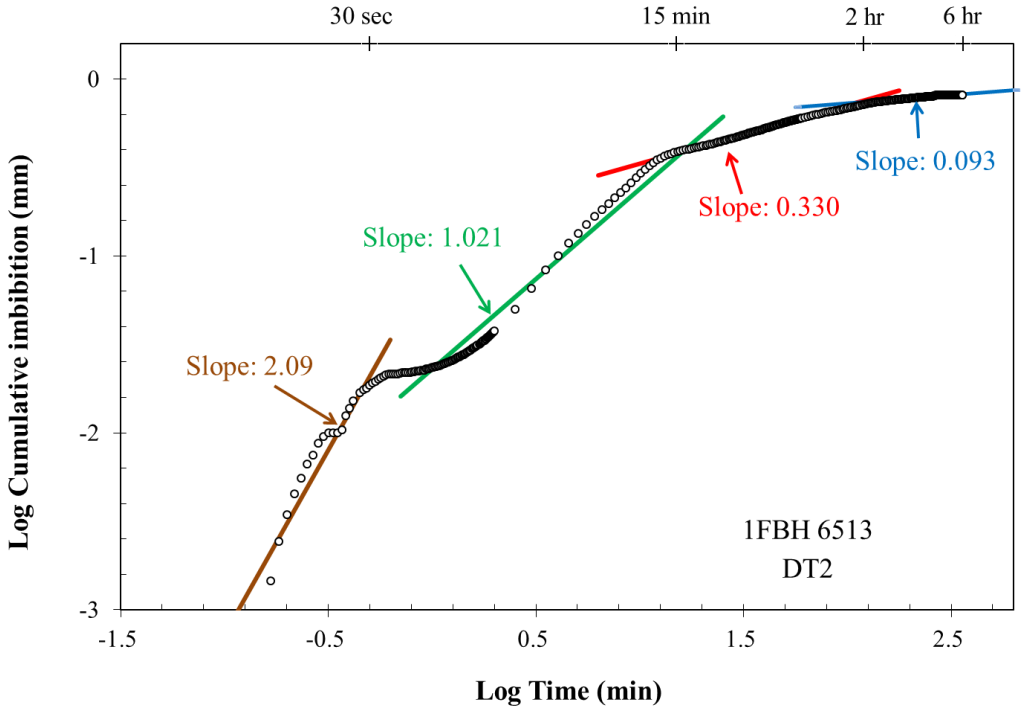

Figure 27: 1FBH 6513 Imbibition graph using DIW (top) and DT2 (bottom)

4.7 Liquid Pycnometry

Liquid pycnometry is used to determine the apparent bulk density of different sample size fractions. Samples 1F 4648 & 4705, 1FBH 6513, and 2RK 4939 & 4981 were tested using DIW , DT2, and THF. Size fractions used for this experiment include GRI+ (1.70 - 2.36 mm), A (841 - 1700 µm), GRI (500 - 841 µm), B (177 - 500 µm), and C (75 - 177 µm). Each size fraction was tested three times using DIW and DT2 and the average was used. The GRI size fraction was only tested using DIW and all samples were only able to be tested one time using THF. The results are shown in Table 10. Most results tend to be erratic, but a trend of a decrease in bulk density can be observed with a decrease in sample size, especially for DT2 and THF in the 1FBH and 2RK samples.

Sample ID	Size designation	Size	Equivalent spherical diameter (µm)	Apparent bulk density (g/cm3)		
				DI Water	DT2	THF
1F 4648	GRI+	1.70 - 2.36 mm	2030	2.647	2.757	2.804
	Size A	841 - 1700 µm	1271	2.650	2.645	2.721
	GRI	500 - 841 µm	671	2.741		
	Size B	177 - 500 µm	339	2.757	2.754	2.722
	Size C	75 - 177 µm	126	2.754	2.553	2.631
1F 4705	GRI+	1.70 - 2.36 mm	2030	2.677	2.625	2.579
	Size A	841 - 1700 µm	1271	2.687	2.666	2.593
	GRI	500 - 841 µm	671	2.723		
	Size B	177 - 500 µm	339	2.634	2.634	2.595
	Size C	75 - 177 µm	126	1.687	2.550	2.632
1FBH 6513	GRI+	1.70 - 2.36 mm	2030	2.672	2.676	2.667
	Size A	841 - 1700 µm	1271	2.656	2.567	2.703
	GRI	500 - 841 µm	671	2.699		
	Size B	177 - 500 µm	339	2.667	2.585	2.608
	Size C	75 - 177 µm	126	2.649	2.460	2.453
2RK 4939	GRI+	1.70 - 2.36 mm	2030	2.681	2.758	2.688
	Size A	841 - 1700 µm	1271	2.712	2.741	2.583
	GRI	500 - 841 µm	671	2.751		
	Size B	177 - 500 µm	339	2.788	2.625	2.657
	Size C	75 - 177 µm	126	2.758	2.511	2.604
2RK 4939	GRI+	1.70 - 2.36 mm	2030	2.673	2.805	2.652
	Size A	841 - 1700 µm	1271	2.708	2.792	2.624
	GRI	500 - 841 µm	671	2.673		
	Size B	177 - 500 µm	339	2.450	2.694	2.603
	Size C	75 - 177 µm	126	2.688	2.588	2.500

Table 10: Liquid pycnometry results

4.8 Production Data

As previously stated, samples from three wells are included in this study. The 3 wells include 1 Foothills AGH state (1F), 1 Fed BH (1FBH), and 2 Richard Knob AEX State (2RK). Unfortunately, no well logs are available for them, but production data can be found using DrillingInfo and the New Mexico Oil Conservation Division (NMOCD) website. Wells 1F and 1FBH both were found to be dry holes and have since been plugged, but 2RK has been producing gas since May 1, 1995 with its last registered producing date at July 1, 2019. It was drilled to a total depth of 5300 feet and the producing intervals are from 4933-4991 feet. Monthly production of gas (Mcf) and water can be seen in Figure 28. The production volume has gone through several cycles over its life span. For example, the annual McF values from 2010-2018 are 8106, 8224, 5956, 7912, 6451, 5110, 4908, 9253, and 7236, respectively with values through seven months of 2019 only at 1972 Mcf.

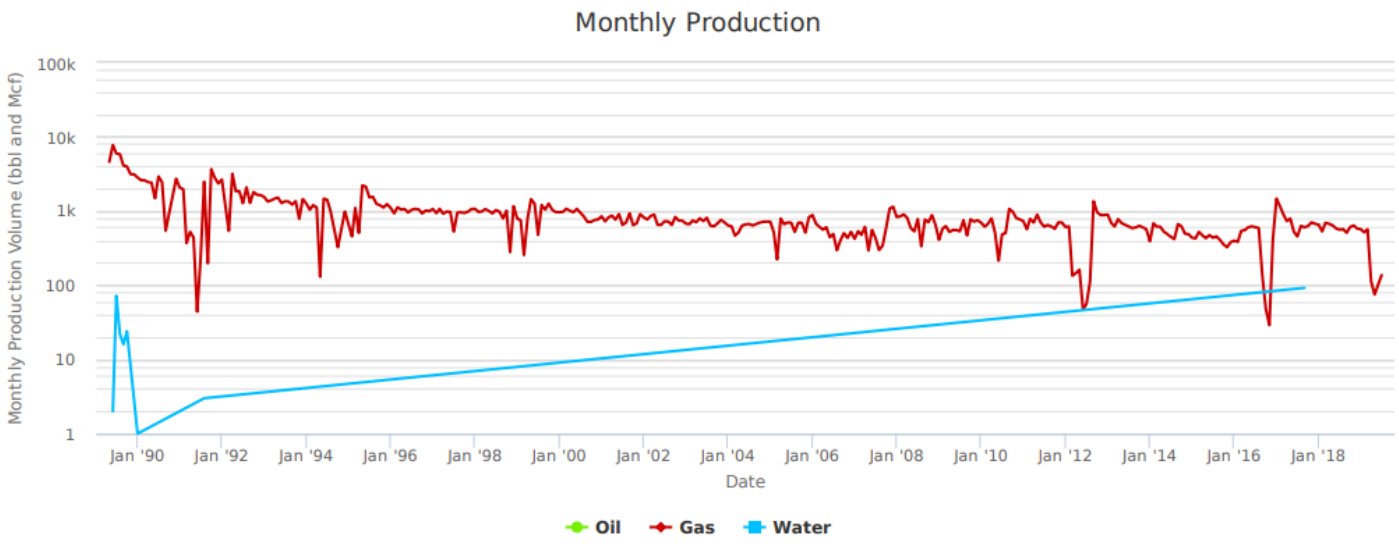

Figure 28: Monthly gas production of 2 Richard Knob AEX State well (DrillingInfo)

Chapter 5: Discussion

5.1 Mineralogy and Geochemistry

The XRD analyses of all samples show that the 1F and 2RK samples are carbonate dominated lithotypes with most of them containing 90%+ (calcite and dolomite). Sample 1FBH 6490, a clay-rich siliceous mudstone, exhibits the highest amounts of quartz, feldspar, and clay, while sample 1FBH 6513, a silica-rich carbonate mudstone, contains 72% carbonate along with 18% (quartz + feldspar) and ~10% clay. The mineral contents can play a significant role in TOC %, in fact Wand and Carr (2013) showed that a correlation between quartz content and TOC % exists; the higher the quartz % is, the higher the TOC % is. Scatter plots are created to show the correlation between mineral content and TOC % (Figure 29) and lithofacies and TOC % (Figure 30). Distinct trends can be seen where an increase in (quartz + feldspar) and clay % coincides with an increase in TOC%, while an increase in carbonate % coincides with a decrease in TOC %.

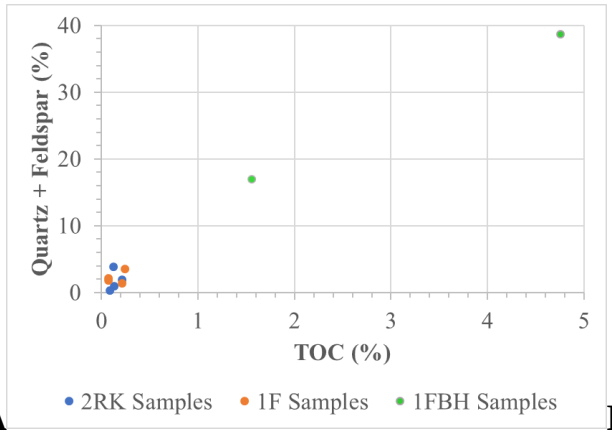

A

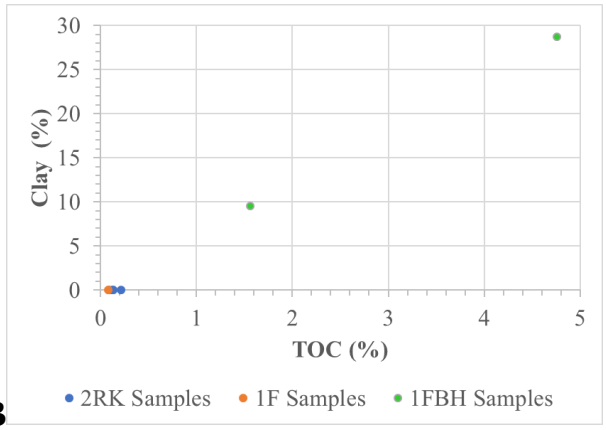

B

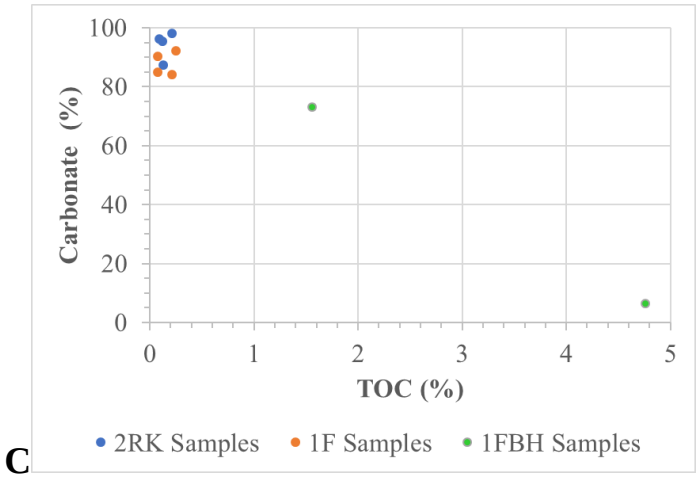

C

Figure 29: Mineral content vs. TOC comparison: A) Quartz + Feldspar; B) Clay; C) Carbonate

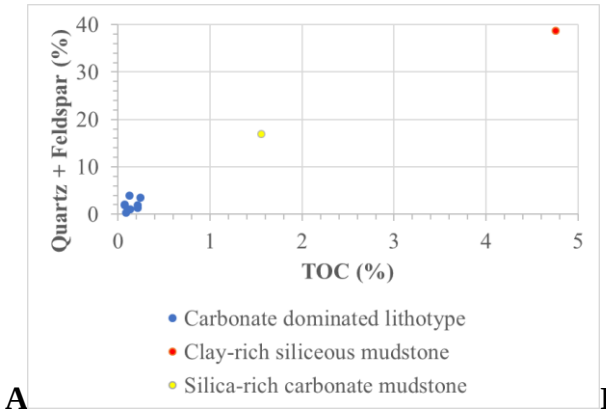

A

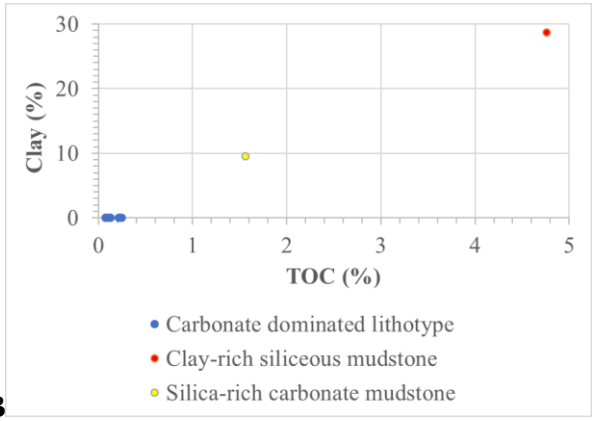

B

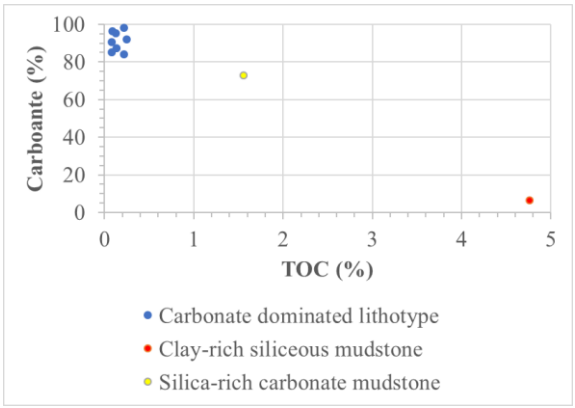

C

Figure 30: Lithofacies vs. TOC comparison: A) Quartz + Feldspar; B) Clay; C) Carbonate

Plotting S1 against TOC% with the oil crossover line proposed by Jarvie (2012) can be a useful tool in determining if a well is expected to produce oil. A similar plot has been used for Wolfcamp samples by Quintero (2016) and Chang (2019). In this study all samples plot below the crossover line of 1:1 for S1 and TOC; note that the coring of these three wells occurred 30 (1F/2RK) and 40 (1FBH) years ago with a loss of hydrocarbons (Figure 31). TOC vs. S2 was shown in Figure 13 and S2/Hydrogen Index vs. Depth in Figure 14. These plots indicate that the kerogen contained within the samples is gas prone. This information is validated by the production data found for well 2 Richard Knob AEX State (2RK) (Section 4.8 and Figure 28**).**

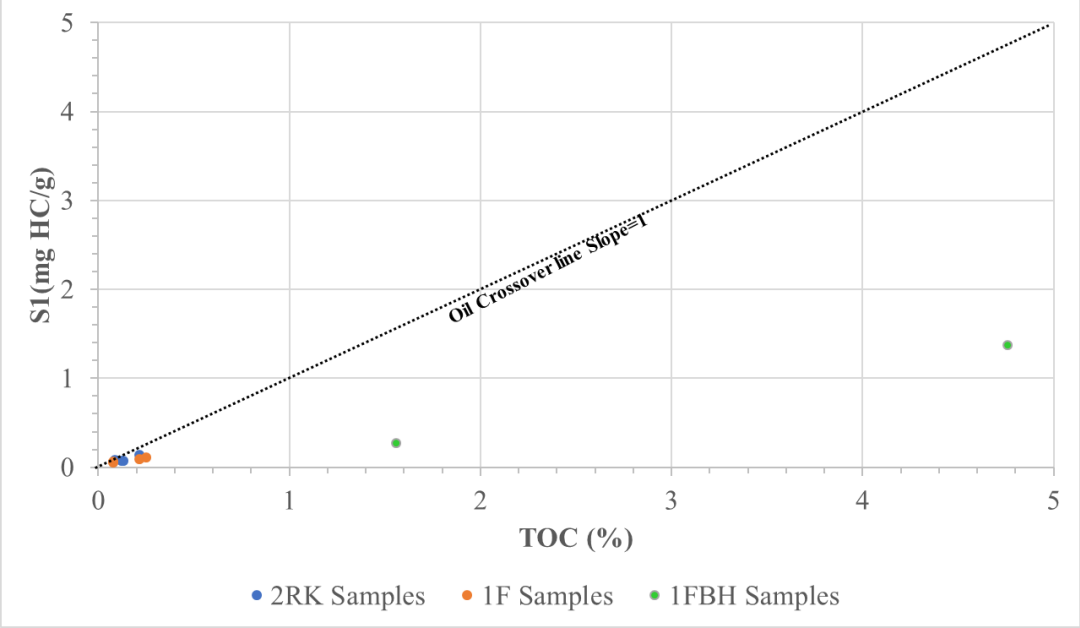

Figure 31: S1 vs. TOC % with oil crossover line of Jarvie (2012).

5.2 Porosity Results from Different Approaches

Both porosity and permeability are vitally important parameters needed to determine fluid storage and migration potential throughout a formation. For this study porosity was

estimated using MIP and vacuum saturation tests. Mercury is the fluid used for MIP while DIW, DT2, and THF were used for vacuum saturation. Porosity values tend to agree fairly well across these two testing procedures (Table 11). For the cubic samples, MIP porosity values range from 0.448-9.74%. Vacuum saturation porosity values range from 0.869-9.80% for DIW, 1.60-10.4% for DT2, and 0.648-9.94% for THF. This agrees with the literature that the porosity values for the Wolfcamp formation typically fall between 2-12% (EIA, 2018). Samples 1F 4648, 2RK 4899, 2RK 4966, and 2RK 4981 do not fall within this range, but all other samples agree with that assessment. Scatter plots are created to show the correlation between porosity % and mineral content (Figure 32). An overall trend of increasing porosity % with increased (quartz & feldspar) and clay %, as well as a decrease in porosity % with increased carbonate %, can be seen. However, the carbonate dominated samples 1F 4693, 1F 4705, and 2RK 4939 exhibit high porosity values and therefore do not follow this trend. The difference can be correlated to their dominant pore-throat network of >100 nm, which contain intergranular pore spaces along with microfractures/laminations. A detailed description of pore-throat network can be seen in the following Section (5.3).

Sample ID	MICP Porosity (%)	Vacuum Saturation Porosity (%)			Average (%)
		DI Water	DT2	THF	
1F 4648	1.004	1.230	1.967	1.436	1.409
1F 4672	N/A	2.309	2.373	1.386	2.023
1F 4693	4.885	5.623	5.705	4.575	5.197
1F 4705	9.745	9.799	10.436	9.937	9.979
1FBH 6490	2.682	3.370	4.377	5.155	3.896
1FBH 6513	N/A	2.531	3.185	2.500	2.739
2RK 4899	0.448	0.869	1.599	0.648	0.891
2RK 4939	7.661	8.673	5.724	8.916	7.744
2RK 4966	N/A	0.985	1.893	0.782	1.220
2RK 4981	0.494	1.317	2.078	1.675	1.391

Table 11: Comparison of MIP and vacuum saturation porosity (%) for cubic samples

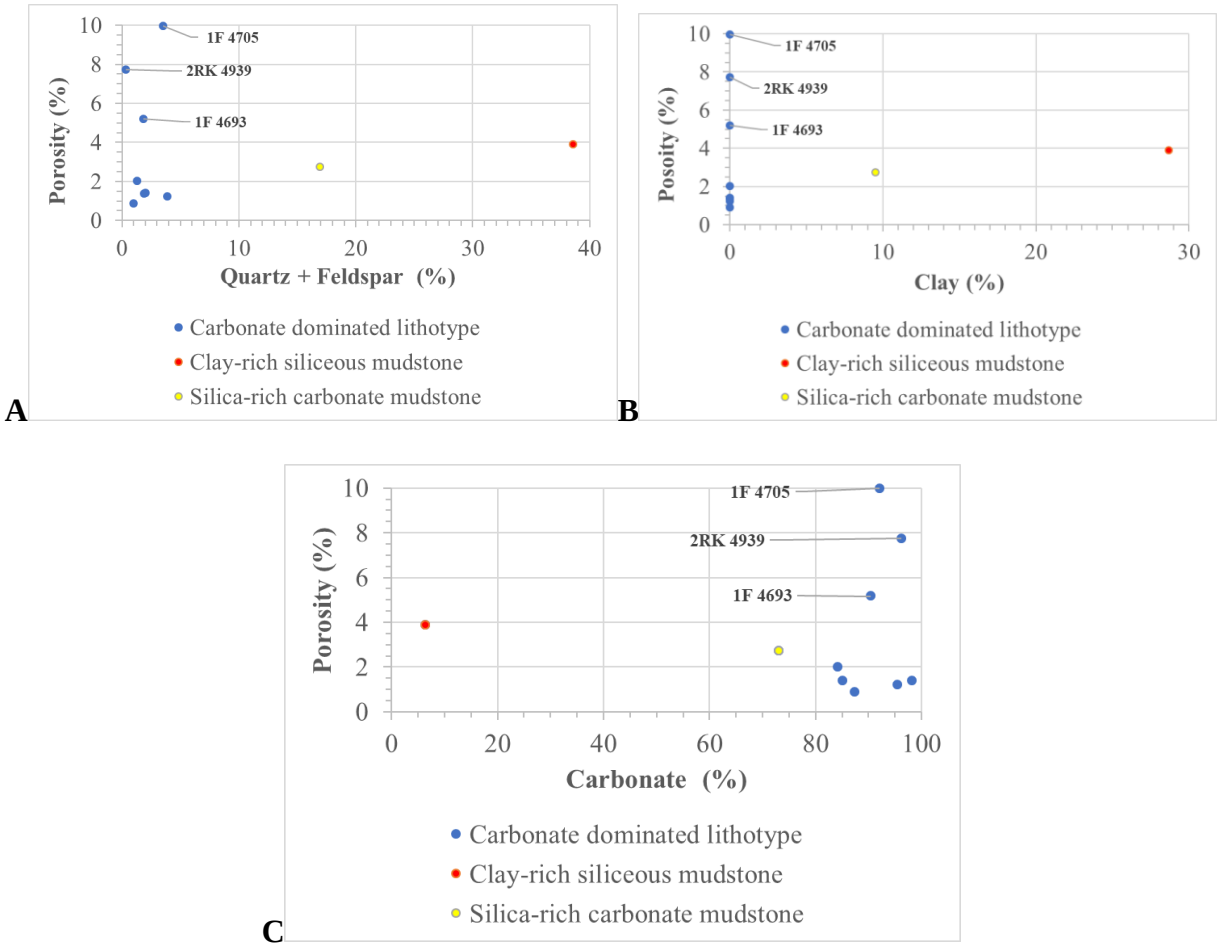

Figure 32: Lithofacies vs. porosity comparison: A) Quartz + Feldspar; B) Clay; C) Carbonate

5.3 Other Pore Structure Parameters

MIP was used to characterize pore structure for this study. Various properties that help model pore structure being quantified include porosity, permeability, tortuosity, and pore-throat size distribution. Permeability for 1FBH 6490, clay-rich siliceous mudstone is 2.75 nD, while permeability ranges from 20.4-5.44×105 nD for the carbonate dominated 1F and 2RK samples (Table 12). All samples show the largest concentration of pores to be intergranular, and 1FBH 6490 shows a fairly high percentage of organic pores (43.47%) and pores between clay grains (21.14%). Results show that the dominant pore network for the samples falls within either the

2.5-50 nm or >100 nm range. Samples 1FBH 6490, 2RK 4981 and 1F 4648 all have dominant pore throat sizes of 2.8-50 nm, while samples 1F 4693, 1F 4705, 2RK 4899, and 2RK 4939 all have dominant pore sizes of >100 nm. Permeability for pore throat sizes of 2.8-50 nm range from 2.75-21.63 nD and the effective tortuosity, a measurement of distance the fluid will travel in a tortuous pathway, ranges from 375-2083. For pore throat sizes >100 nm, permeability ranges from $8.85x10^{3}$-$5.44x10^{5}$ nD and the effective tortuosity ranges from 9.35-295. A distinct trend within the two dominant pore sizes shows that as the pore-throat size decreases, the permeability decreases and tortuosity increases. MIP results for the dominant pore-throat network are presented in Table 12, and MIP results for each pore-throat size are shown in Table 7. The samples tested in this study show much lower permeability values than typically shown for Wolfcamp where lows are estimated to be around 10 mD (EIA, 2018); the difference is expected to lie in the sample size used (containing fractures or not) and detection limits. In addition, the difference could also stem from the fact that 6 out of 7 samples tested are carbonate-dominated lithotypes. A study carried out by Mann (2017) on carbonates of the North West Shelf showed permeability values much closer to what was found in this study. In dolomite dominated samples, he found MIP permeabilities to be 1.73 and 2.12 mD. Samples 1F 4705 (90.9% dolomite) and 2RK 4939 (77.3% dolomite) show similar, although less than one order of magnitude lower, values of 0.544 and 0.330 mD, respectively.

Sample ID	Pore Throat Size (nm)	Bulk density (g/cm3)	Apparent (skeletal) density (g/cm3)	Total pore area (m^2/g)	Porosity (%)	Permeability k (nD)	Effective Tortuosity (D0/De)
1F 4648	2.8-50	2.67	2.70	0.81	1.00	21.63	796.64
1F 4693	>100	2.67	2.81	0.93	4.88	8.85E+03	51.92
1F 4705	>100	2.40	2.66	0.70	9.74	3.30E+05	241.62
2RK 4899	>100	2.74	2.76	0.14	0.45	2.24E+05	9.35
2RK 4939	>100	2.55	2.76	2.53	7.66	5.44E+05	294.67
2RK 4981	2.8-50	2.68	2.70	0.24	0.49	20.36	375.20
1FBH 6490	2.8-50	2.46	2.52	5.08	2.68	2.75	2082.79

Table 12: MIP results of dominant pore-throat network

5.4 Pore Connectivity and Wettability

Pore connectivity and wettability are two highly related properties. For this study pore connectivity was tested using fluid imbibition with DIW and DT2, while wettability was determined using contact angle measurements. Contact angle results in Table 8 show the samples to be oil-wet with an intermediate water wettability. Imbibition results presented in Table 9 show an intermediate (0.25-0.5) pore connectivity when using DIW for all samples, except for 1F 4693 (low connectivity) and 1FBH 6490 (high connectivity). DT2 results show high pore connectivity for all samples, except for 1FBH 6513 and 2RK 4939 which exhibit intermediate pore connectivity. Scatter plots show a comparison of lithofacies vs. connectivity slope for DIW (Figure 33) and DT2 (Figure 34). For DIW, the connectivity slope is shows to be most influenced by the presence of carbonate. Carbonate dominated lithotypes along with the silica rich carbonate mudstone (73% carbonate) exhibits lower values than the clay-rich siliceous mudstone (6.4% carbonate). For DT2 no distinct trend is observed.

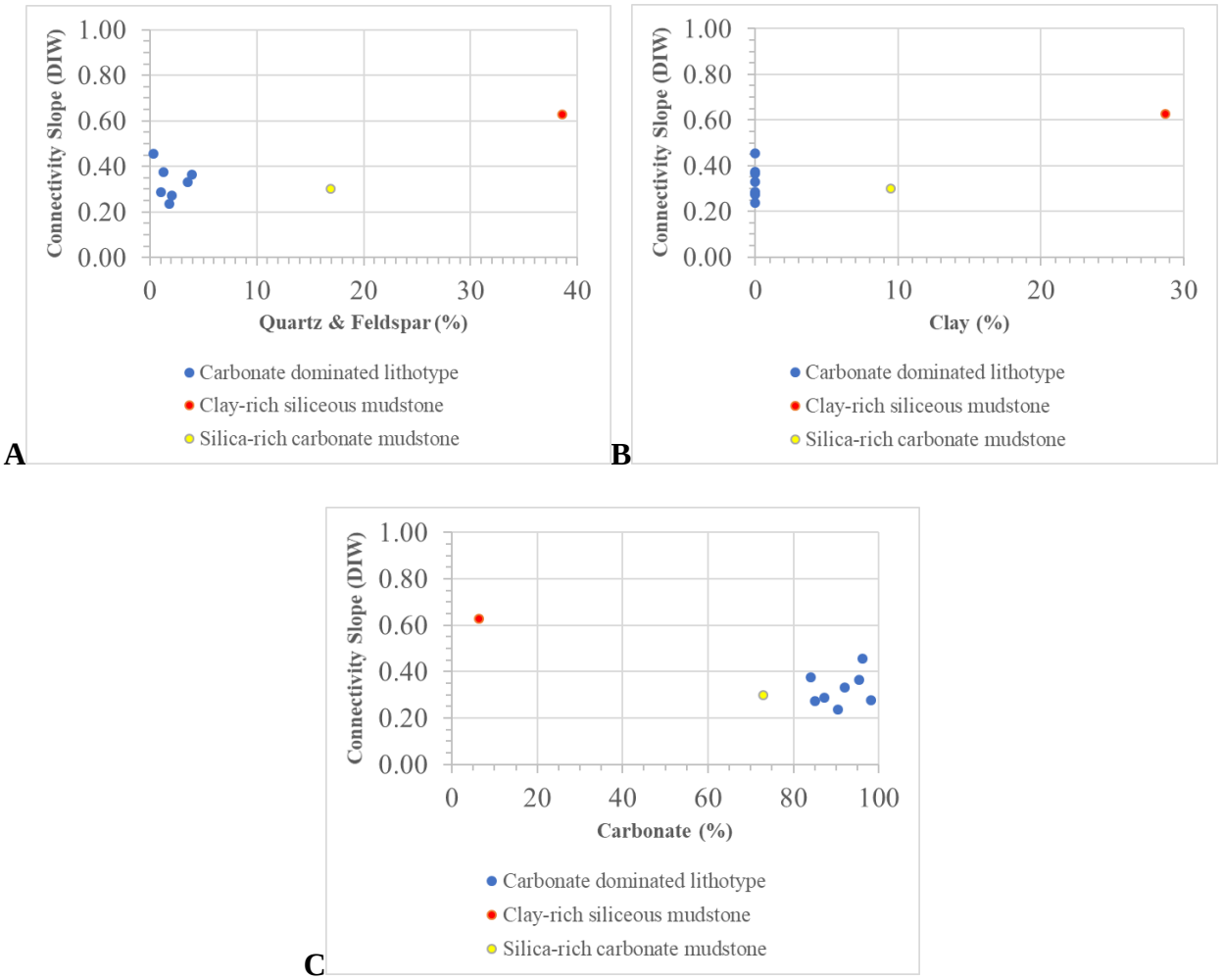

Figure 33: Lithofacies vs. DIW connectivity slope comparison: A) Quartz + Feldspar; B) Clay; C) Carbonate

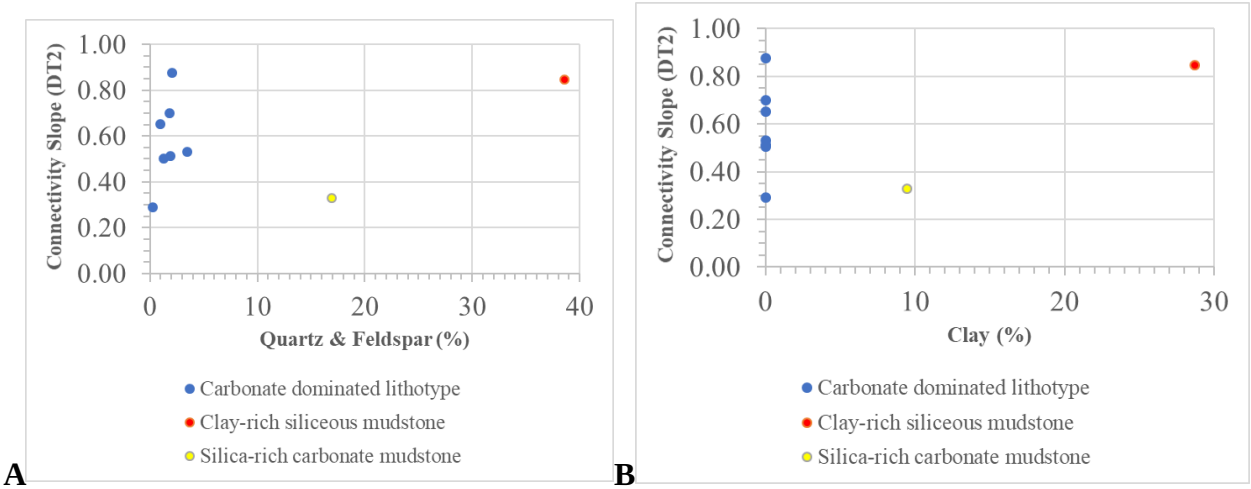

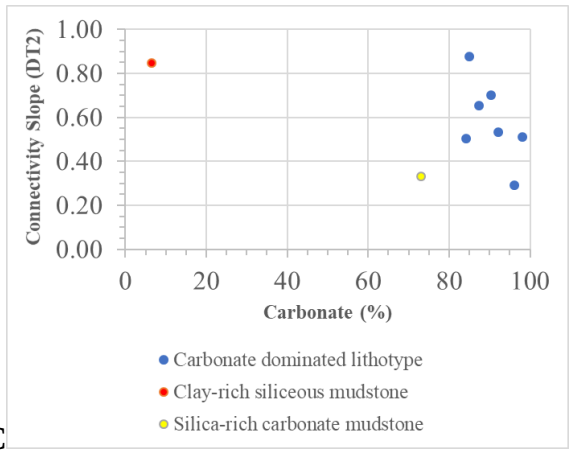

C

Figure 34: Lithofacies vs. DT2 connectivity slope comparison: A) Quartz + Feldspar; B) Clay; C) Carbonate

5.5 Density

Density measurements are another important factor when characterizing nano-petrophysical properties. Density values were calculated using MIP and vacuum saturation with DIW, DT2 and THF. Bulk and grain densities of cubic samples are presented in Table 13. The results agree well with each other with only a small difference in values between fluids. Lithofacies vs. average density measurements for Bulk (Figure 35) and Grain (Figure 36) density show a trend of increase in density with increase in carbonate %.

Sample ID	Bulk Density (g/cm3)				Grain Density (g/cm3)			
	MICP	Vacuum Saturation			MICP	Vacuum Saturation		
		DI Water	DT2	THF		DI Water	DT2	THF
1F 4648	2.670	2.716	2.800	2.665	2.700	2.750	2.856	2.689
1F 4672	N/A	2.774	2.812	2.842	N/A	2.840	2.880	2.882
1F 4693	2.670	2.727	2.781	2.724	2.810	2.890	2.949	2.855
1F 4705	2.400	2.566	2.608	2.550	2.660	2.844	2.912	2.831
1F 6490	2.460	2.493	2.495	2.522	2.520	2.579	2.609	2.659
1F 6513	N/A	2.608	2.638	2.576	N/A	2.676	2.725	2.642
2RK 4899	2.740	2.820	2.881	2.804	2.760	2.856	2.928	2.822
2RK 4939	2.550	2.590	2.721	2.566	2.760	2.795	2.886	2.817
2RK 4966	N/A	2.702	2.749	2.675	N/A	2.729	2.802	2.696
2RK 4981	2.680	2.687	2.722	2.660	2.700	2.723	2.780	2.706

Table 13: Density measurement comparison of MIP and vacuum saturation methods for cubic samples

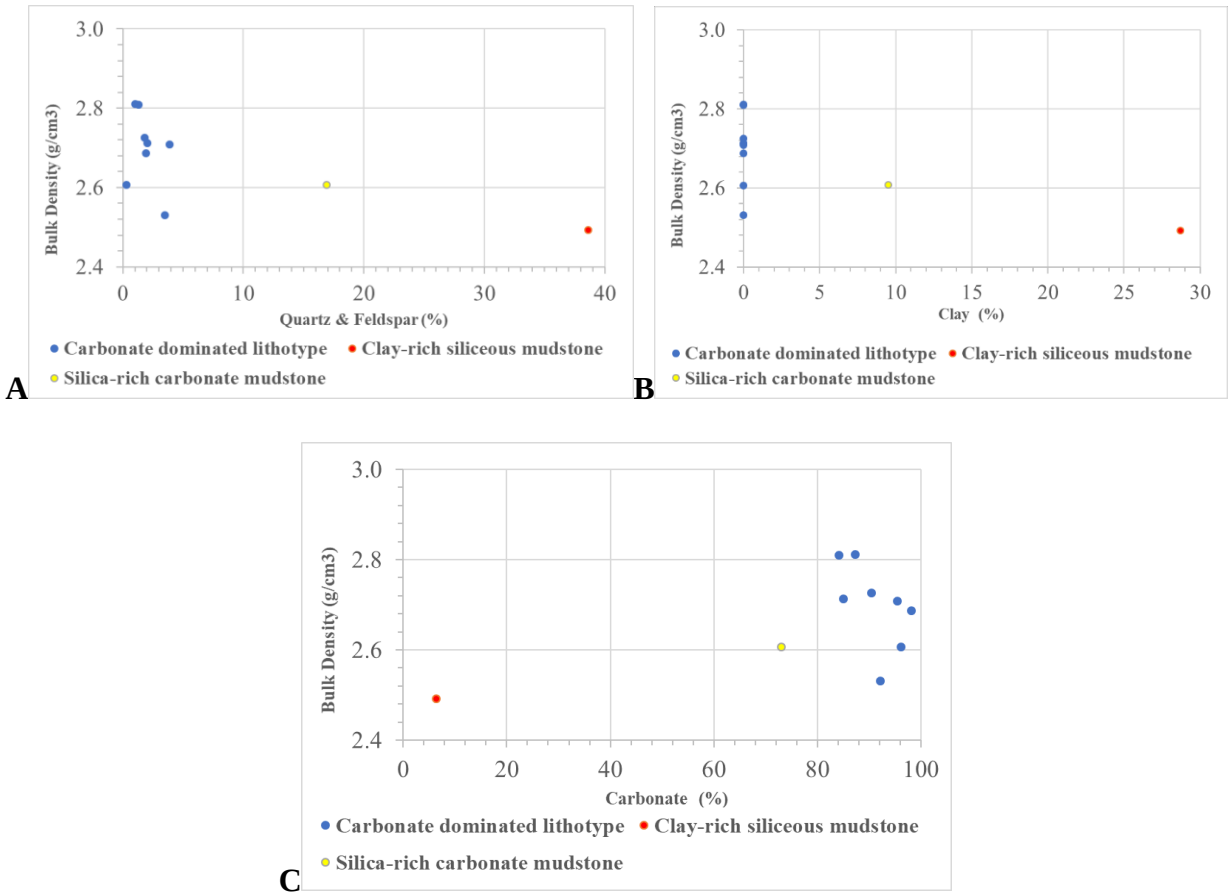

Figure 35: Lithofacies vs. bulk density : A) Quartz + Feldspar; B) Clay; C) Carbonate

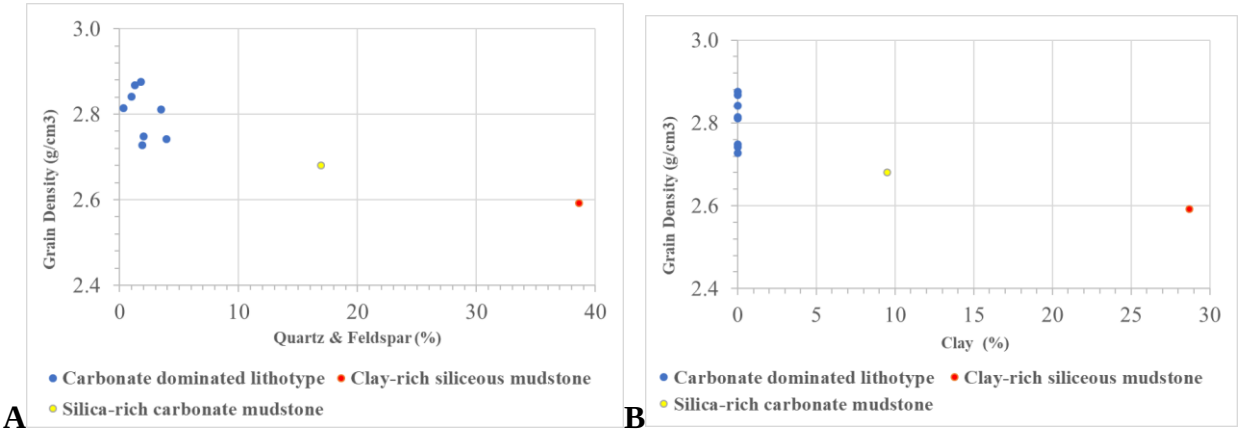

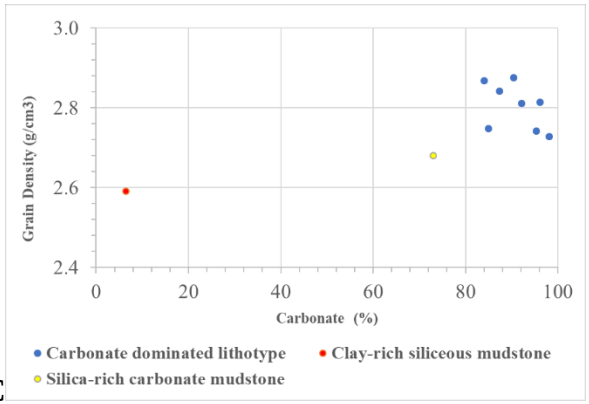

C

Figure 35: Lithofacies vs. grain density : A) Quartz + Feldspar; B) Clay; C) Carbonate

Chapter 6: Conclusions and Recommendations

6.1 Conclusions

The Wolfcamp Formation in the Delaware Basin is one of the most highly productive shale plays in the world. The purpose of this study is to assess the petrophysical properties of the formation for a better understanding of how fluid may flow through it. A total of 10 samples from 3 wells in Eddy County of New Mexico were collected and tested using XRD, pyrolysis, MIP, fluid imbibition, vacuum saturation, liquid displacement, and contact angle measurements. The results from these procedures are as follows:

1) Mineral compositions from XRD analyses show that all 8 samples from 1F and 2RK wells are carbonate-dominated lithotypes (~90% carbonate) while 1FBH 6490 is a clay-rich siliceous mudstone and 1FBH 6513 is a silica-rich carbonate mudstone.
2) TOC percentages show a general trend of increased TOC with quartz and clay content and low percentages within the carbonate samples. Carbonate-rich rocks ranged from 0.09-0.25% TOC, while Clay-rich siliceous mudstone 1FBH 6490

exhibits the highest TOC % at 4.76% as compared to 1.56% for silica-rich carbonate mudstone 1FBH 6513.

3) All samples have a high concentration of intergranular pores and two dominant pore-throat sizes were discovered. Samples 1FBH 6490, 2RK 4981 and 1F 4648 all have dominant pore-throat sizes of 2.8-50 nm, while 1F 4693, 1F 4705, 2RK 4899, and 2RK 4939 all have dominant pore-throat sizes of >100 nm.
4) An obvious trend between dominant pore-throat size, permeability, and tortuosity can be observed. As pore-throat size decreases, permeability decreases while tortuosity increases. Permeability values are highly variable and range from 2.75 nD to 5.44×10^5 nD and tortuosity values range from 9.35 to 2083.
5) Porosity values show a trend of increase with a decrease in sample size, indicating a low pore connectivity characteristics of these fine-grained mudrocks. Edge-accessible porosity of cube-sized samples from vacuum saturation tests ranges from 0.0869-9.80% with DIW, 1.60-10.4% with DT2, and 0.648-9.94% using THF. MIP porosity values range from 0.448-9.74%. An overall trend of increasing porosity% with increased (quartz & feldspar) and clay% and a decrease in porosity% with increased carbonate% can be observed. The high porosity of the carbonate dominated samples 1F 4693, 1F 4705, and 2RK 4939 can be correlated to their dominant pore-throat network containing mostly intragranular pore spaces and microfractures/laminations.
6) Overall pore connectivity is classified as intermediate (0.25-0.50) towards DIW and high (> 0.50) towards DT2. Only two samples show anything other than an intermediate classification for DIW. Sample 1F 4648 exhibits a low connectivity

slope for DIW while clay-rich siliceous mudstone 1FBH 6490 exhibits a high connectivity slope for water. For DT2 samples 1FBH 6513 and 2RK 4939 show intermediate connectivity slopes. A trend is observed for DIW where carbonate dominated lithotypes along with the silica-rich carbonate mudstone exhibits lower values than the clay-rich siliceous mudstone. For DT2, no distinct trend with lithofacies is found.

7) Density measurements obtained using MIP and vacuum saturation tests show a good agreement. The average of bulk and grain densities for the carbonate-rich 1F and 2RK samples range from 2.531-2.811 g/cm^3 and 2.727-2.876 g/cm^3, respectively. Bulk and grain density averages for the 1FBH samples range 2.493-2.607 g/cm^3 and 2.592-2.681 g/cm^3, respectively. A correlation between carbonate% and both density types is present: as carbonate% increases, density values increase.

6.2 Recommendations

Given the enormous size and highly variable lithology of the Wolfcamp Formation, it is recommended that more samples from different locations and depths to be tested using these methods along with others such as field emission-scanning electron microscopy for pore typing and small-angle neutron scattering for total (both edge-connected and isolated) pores. To fully characterize petrophysical properties, one would ideally have well logs to compare to testing results, but no well logs are available even though the 2RK well is a gas producing well. Pairing well log data along with additional testing procedures, such as FE-SEM and SANS imaging for pore characterization, would help to provide a holistic picture of nanopore structure.

References

Becker, S. 2019. Laboratory-Scale Petrophysical Evaluation of Facies Effect On Reservoir Quality & Source Potential and Upscaled Well Log Analysis in the Pennsylvanian-Permian Wolfcamp-Spraberry Intervals, Midland Basin, Texas, USA. M.S. Thesis, the University of Texas at Arlington, USA.

Chang, A. 2019. Nano-Petrophysical Properties of the Bone Spring and the Wolfcamp Formation in the Delaware Basin, New Mexico, USA. M.S. Thesis, the University of Texas at Arlington, USA.

DrillingInfo. 2019. www.drillinginfo.com

EIA (Energy Information Agency), 2018, Permian Basin Wolfcamp Shale Play Geology Review, U.S. Energy Information
Publication report.
https://www.eia.gov/maps/pdf/PermianBasin_Wolfcamp_EIAReport_Oct2018.pdf

Ewing, T. E. 1991, The tectonic framework of Texas: Text to accompany "The Tectonic Map of Texas", Austin, Bureau of Economic Geology, The University of Texas at Austin, 36 pp.

Galley, J. E. 1958, Oil and Geology in the Permian Basin of Texas and New Mexico: North America: Habitat of Oil, AAPG special volume, pp. 395-446.

Gao, Z., & Hu, Q. 2013. Estimating permeability using median pore-throat radius obtained from mercury intrusion porosimetry. Journal of Geophysics and Engineering, 10, 025014. DOI:10.1088/1742-2132/10/2/025014

Gardiner, W. B., 1990, Fault fabric and structural subprovinces of the Central basin Platform: A model for strike - slip movement, in Flis, J. E., and Price. R. C., eds., Permian basin Oil and Gas Fields: Innovative Ideas in Exploration and Development: Mid land. West Tex.as Geological Society, 90-87, pp. 15-27.

Gaswirth, S. B. 2017. Assessment of Undiscovered Continuous Oil Resources in the Wolfcamp Shale of the Midland basin, West Texas, AAPG ACE Proceedings, April 2017.

Handy, L. L. 1960. Determination of effective capillary pressures for porous media from imbibition data. Differential Equations, 219, 75–80.

Hills, J. M. 1985, Structural evolution of the Permian basin of wes1 Texas and New Mexico, in Dickerson, P. W., and Muehlberger, W. R. (eds.), Structure and Tectonics of Trans-Pecos Texas: Mid land, West Texas Geological Society, 85-81 , pp. 89-99.

Hu, Q. H., Ewing, R. P. and Rowe, H. D. 2015. Low nanopore connectivity limits gas production
in Barnett formation, Journal of Geophysical Research: Solid Earth, 120, 8073–8087.

Jarvie, D. M. 2012. Shale resource systems for oil and gas: Part 2—Shale-oil resource systems. Shale reservoirs—Giant Resources for the 21st Century: AAPG Memoir 97, p. 89, doi: DOI:10.1306/13321447M973489.

Katz, A., and Thompson, A. 1987, Prediction of rock electrical conductivity from mercury injection measurements. Journal of Geophysical Research: Solid Earth, v. 92, p. 599-607.

Majeed, M. H. 2014. Static Contact Angle and Large Water Droplet Thickness Measurements with the Change of Water Temperature. Nahrain University, College of Engineering Journal (NUCEJ) v. 17 no.1, p.114-128.

Mann, G. 2017. Petrophysical Properties of the Yeso, Abo and Cisco Formations in the Permian Basin in New Mexico, U.S.A. M.S. Thesis, the University of Texas at Arlington, USA.

Oriel, S. S., Myers, A.D., and Crosby, E. 1967, West Texas Permian basin region, in McKeeand, E. and Oriel, S. (eds.), Paleotectonic investigations of the Permian system in United States, U.S. Geological Survey Professional Paper 515-A, p. 21-64.

Quintero, R.P. 2016. Coupled Geochemical and Nano-Petrophysical Study of The Spraberry-Wolfcamp Trend West Texas, U.S.A. M.S. Thesis, University of Texas at Arlington, USA.

Robinson, K. 1988, Petroleum geology and hydrocarbon plays of the Permian basin Petroleum province West Texas and southeast New Mexico, U.S. Geological Survey Open-File Report 88-450-Z, 53 pp. https://doi.org/10.3133/ofr88450Z

Schlumberger. 2014. sCore Lithofacies Classification Reveals Barnett Shale Reservoir Quality.

Schlumberger Oilfield Glossary. 2018. Geopressure gradient - Schlumberger Oilfield Glossary. Retrieved from https://www.glossary.oilfield.slb.com/en/Terms/g/geopressure_gradient.aspx

State Of New Mexico OCD. 2019.
https://wwwapps.emnrd.state.nm.us/ocd/ocdpermitting/Data/Wells.aspx

USGS (United Stated Geological Survey). 2018. USGS Announces Largest Continuous Oil Assessment in Texas and New Mexico.
https://www.usgs.gov/news/usgs-announces-largest-continuous-oil-assessment-texas and-new-mexico

Wang, Q. 2019. Nano-petrophysics study of Haynesville Shale, East Texas, USA. M.S. Thesis, The University of Texas at Arlington, USA

Wang, S., Javadpour, F., and Feng, Q. H. 2016. Confinement correction to mercury intrusion capillary pressure of shale nanopores. Scientific Reports, 6: 20160, doi: 10.1038/srep20160.

Washburn, E. W. 1921. Note on a method of determining the distribution of pore size in a porous material. Physics, 7, 115–116.

Yang, K.-M., Dorobek, S. 1995. The Permian basin of West Texas and New Mexico: Tectonic history of a "composite" foreland basin and its effects of stratigraphic development, pp. 149-174, 10.2110/pec.95.52.0149.

Yang, R., Guo, X., Yi, J., Fang, Z., Hu, Q., & He, S. 2017. Spontaneous Imbibition of Three Leading Shale Formations in the Middle Yangtze Platform, South China. Energy and Fuels, 31(7), 6903–6916.

Appendix A

Laboratory Methods and Procedures for XRD Analysis at the Shimadzu Center, The University of Texas at Arlington.

MaximaX XRD-7000: Shimadzu X-ray Diffractometer

Sample Preparation

- Prepare your sample by compacting the sample into the sample holder using a glass slide
- Avoid vertical loading by removing excess sample with the edge of the glass slide
- Attempt to make your sample as flat and homogenous as possible; once this is completed your sample is ready to be analyzed.

Power Operations

- Turn the chiller on by pressing the power button (on the face of the chiller), a green light will illuminate.
    - Allow the chiller to sit for ~20 minutes to adjust to the proper temperature.
- Turn the XRD on by pressing the power button on the left hand side. The green power button will illuminate on the front panel of the XRD.

XRD Calibration:

- Locate and open the [PCXRD] program on the desktop. The main "XRD-6100/7000" panel will display.
- Click the [Display and Setup] icon, a "door alarm check" window will pop up. Follow the prompt to open and close the XRD door, once complete click "Close". An "IOcon" window will pop up with the message "Now Calibration! If ready OK", Click "OK".
- The XRD is officially calibrated and ready to process your sample.

Setting Analysis Conditions:

- To set the processing conditions go to the "XRD 6100/7000" panel.
- Click on the [Right Gonio Condition] icon to open the [Analysis Condition Edit Program] window
- Click the blue bar under [Measurement Mode: Standard] to open the [Standard Condition Edit] window.
- Most of the settings in the [Standard Condition Edit] window will be preset. Only a few conditions will need to be changed.
- The following general condition settings will work for a wide array of materials.

It's very important to follow these next steps, double check any settings you change ensuring to follow these guidelines precisely. This will minimize minor mistakes when processing materials and will prevent damage to the detector.

- Scanning condition: Scan Range (deg) = 2°-70° □ Optional Condition: Check the box [Option Enable]
- Beta Attachment: Control Mode: Rotation
  Rotation Speed (rpm): 6
- Slit Condition: Slit Conditions are preset, and must be verified on the XRD to ensure the proper slit sizes match the settings listed under the Slit Conditions.
  - Checking the Slits:
    - Open the XRD door, on the left side of the XRD is the X-ray tube, the Divergence Slit is attached to the left side of the divergence soller slits.
    - On the right hand side will be the detector arm which contains a set of Scattering soller slits, the Scattering Slit faces the sample (Left) and the Receiving Slit faces the detector (Right).
    - If they are not the same sizes as what is preset in the [Slit Condition] box change the slit's so they do match.
  - Standard Slit Settings:
    - Divergence Slit: 1.0°
    - Scattering Slit: 1.0°
    - Receiving Slit: 0.3 mm

- Double check your settings and make sure they are correct, if they are click [OK].
- A [File & Sample Condition Edit] window will display; change the [Group name] to match your destination folder name and change [File name] and [Sample Name] to match your sample name, click [New].
  - Later samples can be created by simply changing the file and sample names and clicking [Modify].
- Click [Close] on the [Standard Condition Edit] window.

Starting the XRD Processing:

- Locate and click the [Right Giono Analysis] icon on the [XRD-6100/7000] panel.
- Your current sample name should appear highlighted blue in the upper portion of the [Right Gonio System: Analysis Condition Edit Program] window. Highlight your sample and click [Append], this adds your sample to the list in the bottom portion of the window labeled [Entry for Analysis], click [Start]. Your sample should appear in the bottom of the [Right Giono Analysis & Spooler Program] window, click [Start] in this window. This officially starts the analysis process.
  - Indicators for Analysis: A clicking sound will come from the XRD when the locking mechanism on sliding door locks. On the face of the XRD a yellow light should illuminate under [X-RAYS ON].
- Leave all software windows open and allow the XRD to process your sample, this should take ~30 minutes.

Completed XRD Processing:

- A complete peak spectrum should appear in the [Right Giono Analysis & Spooler Program] window upon completion.
- The green [Analyzing!] Box should disappear and the yellow [X-RAYS ON] light should turn off.
- If you have more samples to analyze, continue to run your samples in the same manner listed above.

Opening Peak Profile Spectrum:

- Locate and open the icon for the [MDI jade 9] software on the Desktop.
- Under [file], click [Read], locate the folder [xddat] under [favorites]. Locate the folder where your samples are saved.
- In your folder, each sample should have a [.RAW] file, use this file to open your selected spectrum in the [Jade 9] software.

Identifying Minerals in Peak Spectrum:

It's important to have an educated background on the sample you're analyzing. Knowledge regarding the bulk composition and what you're searching for will greatly reduce the amount of time spent IDing the various peaks in the spectrum.

- Locate the [Find Peaks] icon on the main tool bar next to the [Floppy Disk/Save] icon, this will identify and mark any statistically significant peaks within the spectrum
- Choose a mineral database: At the top of the panel to the right of the spectrum window, there will be a drop-down menu choose the [RDB-Minerals] as the database. The RDB-Mineral database should be predominately used to identify most minerals in your spectra.
    - If you cannot find a mineral in the RDB-Minerals database change to the [PDF+4 Minerals] database library, but be sure to change back to the RDB database once the mineral is located.
- Begin searching for minerals based on your pre-existing knowledge regarding the sample. When you identify minerals that fit your peak spectrum hit [Enter] on the keyboard, this process will add the minerals to a compiled list of those minerals which you identified in the spectrum.
- Once you have exhausted your initial hypothetical list of minerals, a helpful tool to use is the [Line Based Search/Match]. Go to the main tool bar and locate [Identify] and select the [Line Based Search] option.
    - This tool will compile a list of minerals by searching a selected PDF database for entries with peaks which are statistical matches for the peaks identified within your spectrum.
    - Settings:
        - [Two-Theta Error Window] max setting should be no more than 0.24%
        - [Top Hits to List] max setting 80
    - Set the parameters and click the blue [Play] icon next to the [X] to run the search and generate a list of possible phases that might fit your spectra. *Note: the linebased search should not be used as a primary way to identify the bulk mineral mode of the sample as the software is not consistent when generating phases and will possibly leave out important phases for the spectrum*.

Model Analysis:

- Once all minerals have been ID'd, check that they have been added to the mineral list by pushing [Enter] on the keyboard.
- Click the [%] icon next to the drop-down mineral list located on the toolbar in the middle of the window to begin modal analysis.
    - An overlay will appear with different chart configurations of the modal results, to change the configurations of the chart use the drop-down menu in the chart window.
- To view the modal analysis in text format: locate and click the […] icon near the [%] icon. This will list the minerals by name, chemical formula, and the normalized weight percent for each mineral. It will also state if the mineral is a [major], [minor], [trace], or [absent] component in the sample.
- If you would like to remove a mineral from your mineral list at any time, highlight the mineral and press [Delete] on the keyboard. [Absent] phases should be removed from the list by this method.

Analysis Check with Pattern Deconvolution:

- A key indication that the peak spectrum has been fully fitted and identified is by using the [Pattern Deconvolution] tool which automatically runs with the modal analysis.
    - The pattern deconvolution tool will generate a red overlay spectrum on top of the original white spectrum.
    - This process is generating a [Best Fit Profile] composed of the selected mineral standards from the [Mineral PDF database library] with your sample spectrum.
    - If all minerals have been properly identified, then the red deconvolution overlay will match the peak spectra for each peak. If there are peaks that don't have the red deconvolution overlay then those peaks have not been identified.
- Continue processing your spectrum until your original spectra and the deconvolution spectra match.

Saving Data:

To save your data,

- Go to [file] and [Save], save your data under [Current work as *.SAV]. This will save all analysis as a separate file.

Appendix B

Laboratory Methods and Procedures for Total Organic Carbon and Pyrolysis Analysis at

GeoMark Research

Procedures – GeoMark Research, LLC.

1. Sample Requirements for a Typical Geochemical Program

For geochemical analysis a teaspoon (ca. 10 g.) of sample material is needed when TOC, RockEval, vitrinite reflectance and residual hydrocarbon fluid fingerprinting is to be completed. If possible, a tablespoon is preferred. However, it is possible to complete a detailed program with even less sample, although there is dependency on the sample characteristics (e.g., organic richness, abundance of vitrinite, amount of staining). Sample prep includes grinding the sample with mortar and pestle until it passes through a 60-mesh sieve.

2. Total Organic Carbon (TOC) – LECO C230 instrument

Leco TOC analysis requires decarbonation of the rock sample by treatment with hydrochloric acid (HCl). This is done by treating the samples with Concentrated HCl for at least two hours. The samples are then rinsed with water and flushed through a filtration apparatus to remove the acid. The filter is then removed, placed into a LECO crucible and dried in a low temperature oven (110 C) for a minimum of 4 hours. Samples may also be weighed after this process in order to obtain carbonate% based on weight loss.

The LECO C230 instrument is calibrated with standards having known carbon contents. This is completed by combustion of these standards by heating to 1200°C in the presence of oxygen. Both carbon monoxide and carbon dioxide are generated, and the carbon monoxide is converted to carbon dioxide by a catalyst. The carbon dioxide is measured by an IR cell. Combustion of unknowns is then completed and the response of unknowns per mass unit is compared to that of the calibration standard, thereby the TOC is determined.

Standards are analyzed as unknowns every 10 samples to check the variation and calibration of the analysis. Random and selected reruns are done to verify the data. The acceptable standard deviation for TOC is 3% variation from established value.

3. Rock Eval / HAWK Pyrolysis

Approximately 100 mg of washed, ground (60 mesh) whole rock sample is analyzed in the Rock-Eval or HAWK instrument. Organic rich samples are analyzed at reduced weights whenever the S2 value exceeds 40.0 mg/g or TOC exceeds 7-8%. Samples must be re-analyzed at lower weights when these values are obtained at 100 mg.

RE-II Operating Conditions

S1: 300^{o}C for 3 minutes
S2: 300^{o}C to 550^{o}C at 25^{o}C/min; hold at 550^{o}C for 1 minute
S3: trapped between 300 to 390^{o}

RE-VI Operating Conditions

S1: 300^{o}C for 3 minutes
S2: 300^{o}C to 650^{o}C at 25oC/min; hold at 650^{o}C for 0 minute
S3: measured between 300 to 400^{o}

HAWK Operating Conditions

S1: 300^{o}C for 3 minutes
S2: 300^{o}C to 650^{o}C at 25oC/min; hold at 650^{o}C for 0 minute
S3: measured between 300 to 400^{o}

Measurements from Rock-Eval are:

S1: free oil content (mg HC/g rock)
S2: remaining generation potential (mg HC/g rock)
T_{max}: temperature at maximum evolution of S2 hydrocarbons (^{o}C)
S3: organic carbon dioxide yield (mg CO_2/ g rock)

Several useful ratios are also utilized from Rock-Eval and TOC data. These are:

Hydrogen Index (HI):	S2/TOC x 100 (in mg HC/g TOC)
Oxygen Index (OI):	S3/TOC x 100 (in mg CO_2/g TOC)
Normalized Oil Content:	S1/TOC x 100 (in mg HC/g TOC)
S2/S3	
Production Index (PI):	S1/ (S1+S2)

Instrument calibration is achieved using a rock standard. Its values were determined from a calibration curve to pure hydrocarbons of varying concentrations. This standard is analyzed every 10 samples as an unknown to check the instrument calibration. If the analysis of the

standard ran as an unknown does not meet specifications, those preceding data are rejected, the instrument recalibrated, and the samples analyzed again. However, normal variations in the standard are used to adjust any variation in the calibration response. The standard deviation is considered acceptable under the following guidelines:

T_{max}: +/- 2°C
S1: 10% variation from established value
S2: 10% variation from established value
S3: 20% variation from established value

Analytical data are checked selectively and randomly. Selected and random checks are completed on approximately 10% of the samples. A standard is analyzed as an unknown every 10 samples.

4. Turnaround Time:

The standard turnaround time for sample orders over the past 12 months is approximately 2 to 3 weeks, depending on number of samples in the order.